



# Modeling advection in geophysical flows with particle level sets

H. Samuel

*Bayerisches Geoinstitut, Universität Bayreuth, D-95440 Bayreuth, Germany*

M. Evonuk

*Department of Theoretical Physics I, Universität Bayreuth, D-95440 Bayreuth, Germany*

[1] We have applied, for the first time in geodynamical flows, the Particle Level Set method for advecting compositional fields with sharp discontinuities. This robust and efficient Eulerian-Lagrangian technique is based on the concept of Implicit Surfaces, which allows the use of high order accurate numerical schemes in the vicinity of discontinuities. We have tested the Particle Level Set method against the robust and popular Tracer-in-Cell method on well-known 2D thermochemical benchmarks and typical 3D convective flows. The use of Lagrangian tracers in the Particle Level Set method yields accurate solutions of purely advective transport, where sub-grid scale features can be resolved. In every case we ran we found that the Particle Level Set method accuracy equals or is better than the popular Tracer-in-Cell method, and can lead to significantly smaller computational cost, in particular in three-dimensional flows, where the reduction of computational time for modeling advection processes is most needed.

**Components:** 12,700 words, 21 figures, 1 table.

**Keywords:** advection; level set method; numerical modeling; interface tracking; geophysical flows; particle-in-cell method.

**Index Terms:** 0545 Computational Geophysics: Modeling (1952, 4255); 8120 Tectonophysics: Dynamics of lithosphere and mantle: general (1213); 1956 Informatics: Numerical algorithms.

**Received** 15 February 2010; **Revised** 4 June 2010; **Accepted** 10 June 2010; **Published** 21 August 2010.

Samuel, H., and M. Evonuk (2010), Modeling advection in geophysical flows with particle level sets, *Geochem. Geophys. Geosyst.*, 11, Q08020, doi:10.1029/2010GC003081.

## 1. Introduction

[2] Advection is one of the major processes that commonly occurs on various scales in Geodynamics. When diffusion is negligible this transport mode, in its simplest form, can be described by the following differential equation:

$$\frac{\partial C}{\partial t} + \mathbf{U} \cdot \nabla C = 0, \quad (1)$$

where  $t$  is the time, and  $C$  is a scalar quantity (e.g., temperature or a chemical component) being advected by a given velocity field  $\mathbf{U}$ . Various geodynamic scenarios of current interest involve the presence of sharp discontinuities in  $C$  (e.g., core formation processes [Hoink *et al.*, 2006; Samuel *et al.*, 2010; Lin *et al.*, 2009; Monteux *et al.*, 2009; Ichikawa *et al.*, 2010], subduction dynamics [Schmeling *et al.*, 2008; van Hunen *et al.*, 2004], lithospheric dynamics [Muehlhaus *et al.*, 2002],

mantle convective stirring [Manga, 1996; Schmalzl et al., 1996; Tackley, 2002; Samuel and Farnetani, 2003; van Keken et al., 2003; Farnetani and Samuel, 2003], thermochemical plume dynamics [Farnetani and Samuel, 2005; Lin and van Keken, 2005, 2006; Samuel and Bercovici, 2006], multi phase flows in magma chambers [Verhoeven and Schmalzl, 2009], salt diapirism [Weinberg and Schmeling, 1992; Chemia et al., 2008] or bubble dynamics in magma flows [Manga and Stone, 1994]). Unfortunately in such cases, solving for equation (1) can be very challenging because sharp discontinuities lead to numerical instabilities, which prevent the local use of high order numerical schemes.

[3] Several approaches have been used in computational geodynamics in order to overcome this difficulty with variable amounts of success. Despite the use of correcting filters or non-oscillatory, shock-preserving schemes, Eulerian (fixed grid) techniques generally suffer from artificial numerical diffusion and dispersion. Lagrangian approaches (dynamic grids or particles) tend to be more popular in computational geodynamics because they are not prone to excessive numerical diffusion. However, these approaches are generally computationally expensive, especially in 3D, and can suffer from spurious statistical noise.

[4] As an alternative to these aforementioned approaches, a powerful hybrid Eulerian-Lagrangian Particle Level Set method for modeling advection of sharply varying quantities, has become increasingly popular in the field of computer graphics [Enright et al., 2002]. This Particle Level Set method is an extension of the Level Set method [Osher and Sethian, 1988], which is based on the concept of implicit surfaces that mark the boundary between sharply varying scalar fields.

[5] This paper aims to apply this recent method that combines the best of Eulerian and Lagrangian approaches, to geodynamic flows. In the first part of the paper the Particle Level Set methodology is described. In the second part of the paper the method is tested against well known benchmarks and classical two- and three-dimensional Geodynamic flows.

## 2. Numerical Strategies for Advecting a Scalar Field

[6] In this section we first briefly review the numerical methods that have been developed and

commonly used in Geodynamics to solve equation (1). Next we will introduce two relatively recent methods that have proven to be accurate and efficient for advecting sharp material surfaces: the Eulerian Level Set method [Osher and Sethian, 1988] and the Particle Level Set method, a Lagrangian extension of the Level Set approach [Enright et al., 2002]. The pure Eulerian Level Set method is becoming increasingly common in Geodynamics [Gross et al., 2007; Suckale et al., 2010], and the Particle Level Set is a popular method in hydrodynamics and computer graphics [Osher and Fedkiw, 2003]. However, to our knowledge, the Particle Level Set method has not been applied to geodynamic flows.

### 2.1. Popular Advection Methods in Geodynamics

[7] Numerical methods for modeling advective transport can generally be cast into either Eulerian (i.e., fixed grid), Lagrangian (i.e., mobile grid or particles) approaches, or a combination of the two.

#### 2.1.1. Eulerian Methods

[8] The advection equation (1) can be straightforwardly discretized onto a fixed grid. The advantage, in computational geodynamics, is that often the discretization of equation (1) is similar to that of other conservation equations, such as the conservation of energy, which are also discretized on Eulerian grids. Sharp variations in  $C$  require special care in discretizing equation (1). For instance, it is well known that discretizing the advective terms in equation (1) with a second order centered finite difference scheme can lead to the appearance of unphysical spurious oscillations in  $C$  [Press et al., 1992; Fletcher, 1991]. Low order schemes, such as upwinding, provide a way to solve equation (1) without producing oscillations in  $C$ , but are generally prone to significant numerical diffusion. An alternative approach is to add a small diffusion term in equation (1) [Farnetani and Richards, 1995; van Keken et al., 1997] which artificially smoothes  $C$ . Further significant reduction of numerical diffusion can also be achieved with the use of correcting filters [Lenardic and Kaula, 1993; Tackley and King, 2003] and the use of anti-diffusive corrections [Smolakiewicz, 1984].

[9] More sophisticated Eulerian advection schemes have been developed in the past decades. In particular the use of Total Variation Diminishing schemes with flux limiters [Harten, 1984; Sweby,

1984; Roe, 1986] allow a high order discretization of advection in regions where  $C$  varies smoothly and low order monotone discretization of advection in regions where  $C$  varies sharply. Providing that the resolution is sufficient, TVD schemes with flux limiters such as Superbee or Sweby [Roe, 1986], yield significant reduction in numerical diffusion [Ricard *et al.*, 2009; Monteux *et al.*, 2009].

[10] Another approach, popular in hydrodynamic modeling, is to discretize equation (1) using Essentially Non Oscillatory (ENO) and Weighted Essentially Non Oscillatory (WENO) schemes [Harten *et al.*, 1987; Liu *et al.*, 1994]. Such schemes use polynomial interpolation of the discrete values of  $C$ , which upon differentiation yield stencils for the approximation of numerical fluxes. The main idea behind these schemes is the use of either the smoothest local stencil (for ENO schemes) or a weighted combination of local stencils (for WENO schemes), leading to monotonicity even in the vicinity of discontinuities, and high accuracy wherever  $C$  is smooth.

[11] Despite all these improvements, due to the fixed nature of the grid, numerical diffusion and dispersion in Eulerian grids cannot be completely removed [e.g., van Keken *et al.*, 1997; Tackley and King, 2003] and are always significantly larger in regions where  $C$  varies sharply.

[12] Finally, considering a total number of Degrees of Freedom (grid cells/points)  $N$ , and assuming optimum solvers (e.g., multigrid) or explicit schemes are used for solving and discretizing equation (1), the computational cost associated with the use of Eulerian methods goes as  $\sim N$ .

### 2.1.2. Lagrangian (Tracer) Methods

[13] A fundamentally different approach to solve equation (1) can be adopted using Lagrangian methods that involve either the use of deformable meshes or tracer particles that are advected in a given velocity field  $\mathbf{U}$  [Christensen and Hofmann, 1994; van Keken *et al.*, 1997; Samuel and Farnetani, 2003; Tackley and King, 2003]. In this case the Lagrangian version of equation (1) is a set of ordinary differential equations for each component of the particle position vector  $\mathbf{x}_p$

$$\frac{d\mathbf{x}_p}{dt} = \mathbf{U}, \quad (2)$$

which can be integrated using classical methods, e.g., Runge-Kutta of second order or higher. The tracers

locations  $\mathbf{x}_p$  are then converted into a continuum field  $C$  at each time step by weighted averaging [Tackley and King, 2003; Gerya and Yuen, 2003; Deubelbeiss and Kaus, 2008]. The major advantage of Tracer-in-Cell methods (also named tracer ratio methods) is the fact that numerical diffusion is negligible. In addition they allow sub grid scale resolution. On the other hand, these methods suffer from spurious statistical noise because the number of particles is finite. Reducing this noise to an acceptable level requires the use of at least  $3^n$  tracers per cell, where  $n$  is the number of spatial dimensions. This makes these methods computationally expensive, particularly in 3D. Indeed, for the least favorable case (tracers particles located everywhere in the computational domain), the cost associated with the use of Lagrangian methods goes as  $N \times N_{\text{tracer/cell}}$ , where the minimum number of tracers per cell  $N_{\text{tracer/cell}}$  is typically 9 in 2D and 27 in 3D geometry. This leads to an extra cost that can be one or two orders of magnitude larger than the computational cost associated with Eulerian advection methods. In addition, the advection of tracer particles may lead to incorrect results when characteristics are merging [Enright *et al.*, 2002]. Finally, the use of tracer particles is not suitable for numerically determining geometrical quantities such as normal vectors to interfaces or the interface curvature, even in the case of a continuous interface with a smooth curvature.

[14] Other Lagrangian methods focus on tracking only the interface  $\Omega$  that marks changes/discontinuities in the scalar field  $C$ . For instance 2D marker chains have been proven to track accurately the evolution of 2D surfaces [van Keken *et al.*, 1997; Lin and van Keken, 2005; Samuel and Bercovici, 2006], and subdivision surfaces have been successfully applied to 3D geodynamic flows [Schmalzl and Loddoch, 2003]. However, these methods can become prohibitively expensive, even in 2D, because their associated computational cost increases with the area of the interface tracked. Contrary to Tracer-in-Cell methods for which the number of tracers remains constant during the calculation, the area of the interface tracked can grow without bounds. This can lead to a significant increase in computational cost, sometimes exceeding by far the cost associated with advection using Tracer-in-Cell methods [van Keken *et al.*, 1997]. For instance, in chaotic convective flows, the repeated action of stretching and folding leads to efficient convective stirring where the area of the interface  $\Omega$  and consequently the computational cost will grow exponentially with time.

## 2.2. Dynamic Implicit Surfaces for Advecting Sharply Varying Quantities

[15] In the following sections, the Level Set and Particle Level Set methods will be summarized. For more details the reader is referred to *Osher and Sethian* [1988], *Sethian* [1999], *Enright et al.* [2002], *Osher and Fedkiw* [2003] and references therein.

### 2.2.1. Level Set Method

[16] In order to track the location of an interface that marks sharp discontinuities in an advected field  $C$ , *Osher and Sethian* [1988] have developed an Eulerian method whose basic principle consists in the use of an implicit surface, as part of a smooth Level Set function  $\phi$  of higher dimension, which replaces  $C$  in equation (1):

$$\frac{\partial \phi}{\partial t} + \mathbf{U} \cdot \nabla \phi = 0. \quad (3)$$

[17] The choice of the Level Set function is free as long as  $\phi$  remains continuous. However, it is convenient to maintain the Level Set as a signed distance function to the interface  $\Omega$ . This guarantees that  $\phi$  remains smooth and it enables a straightforward reconstruction of the interface  $\Omega$  as it corresponds exactly to the location of the zero level set  $\Omega \equiv \phi = 0$ . A major advantage of the Level Set method over other Eulerian methods lies in the smoothness of  $\phi$ , for which high order accurate schemes can be efficiently applied, thus significantly reducing numerical errors.

[18] When solving equation (3) with physical velocities  $\mathbf{U}$  (i.e., obtained by solving the Navier-Stokes equations) to advect  $\phi$ , the Level Set will be distorted by the flow, therefore, in general,  $\phi$  will not remain a signed distance function to the interface  $\Omega$ . In order to remain a signed distance function, the Level Set function must be reinitialized to meet the following Eikonal requirement at each time step:

$$|\nabla \phi| = 1. \quad (4)$$

[19] However, as proposed by *Sussman et al.* [1994], the Level Set reinitialization step can also be achieved by solving the following non-linear hyperbolic equation to steady state:

$$\frac{\partial \phi}{\partial \tau} = S(\phi_0)(1 - |\nabla \phi|), \quad (5)$$

where  $\phi_0$  is the Level Set determined with equation (3) prior to reinitialization,  $\tau$  represents a fictitious time and  $S(\phi_0)$  is a smoothed signed distance function:

$$S(\phi_0) = \frac{\phi_0}{\sqrt{\phi_0^2 + \varepsilon^2}}, \quad (6)$$

where  $\varepsilon$  is taken as the grid spacing  $\Delta h$  (assuming a constant grid spacing). Note that solving for equation (5) is not computationally prohibitive as the steady state is generally reached within 1 to 2 fictitious time iterations, with a time step  $\Delta \tau = 0.1 \Delta h$  [*Sussman et al.*, 1994]. Similarly to *Sussman et al.* [1994] and *Min and Gibou* [2007], the spatial derivatives in equation (5) can be approximated with a monotone second order Godunov-Hamiltonian scheme. The time discretization of equation (5) is performed via a second order TVD Runge-Kutta (predictor-corrector) scheme [*Shu and Osher*, 1988; *Min and Gibou*, 2007].

[20] As noted by *Sussman et al.* [1994] such a reinitialization step tends to produce artificial displacement of the zero Level Set, which leads eventually to weak mass conservation of the Level Set method. In fact the reinitialization step could be avoided by constructing extension velocities [*Adalsteinsson and Sethian*, 1999; *Sethian*, 1999] for advecting the Level Set when solving equation (3). This has the advantage that the Level Set is not distorted and therefore no reinitialization is necessary. However, the use of tracers in the Particle Level Set method prevents the artificial displacement of the zero Level Set during the reinitialization step. Thus, for simplicity we do not construct extension velocities and maintain the Level Set as a signed distance function by solving equation (5).

[21] Finally, in cases where the velocity field is affected by  $C$ , the Level Set needs to be converted into a compositional field  $C$  as follows:

$$C = \begin{cases} 1 & \text{if } \phi > +l \\ 0 & \text{if } \phi < -l \\ C_i & \text{if } |\phi| \leq l \end{cases} \quad (7)$$

where  $l$  represents the half grid cell diagonal length (e.g., in 3D Cartesian geometry  $l = 0.5 \sqrt{\Delta x^2 + \Delta y^2 + \Delta z^2}$ ).  $C_i$  corresponds to the value of the compositional field in cells that are crossed by the zero Level Set. This quantity can be calculated as the volume fraction of positive  $\phi$  to negative  $\phi$  contained in the cell following, for instance, the approach described by *Sussman and Puckett* [2000] or *Ménard et al.* [2007].

[22] Overall, despite the additional computational cost involved in the reinitialization or the con-

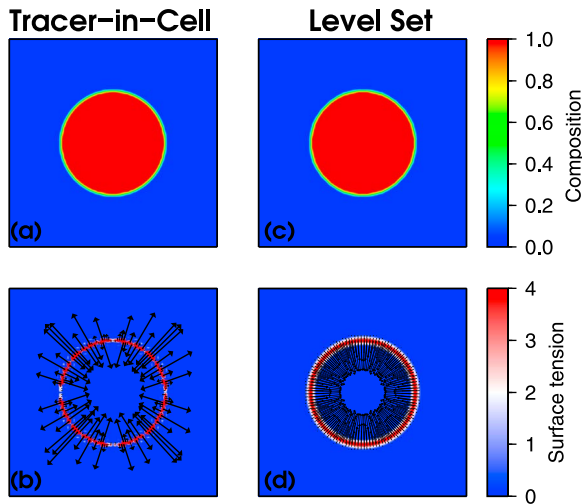


**Figure 1.** Comparison between the (a and b) Tracer-in-Cell and (c and d) Level Set methods. Compositional field  $C$  (Figures 1a and 1c) and surface tension (Figures 1b and 1d) vectors and magnitude of a static, disk-shaped, heterogeneity in a 2D square domain discretized using  $100 \times 100$  identical cells.

struction of extension velocities, the Level Set method is computationally efficient. Indeed, similar to the other Eulerian methods listed in section 2.1.1, the computational cost is  $O(N)$ . However, this limit is an upper bound as equations (1), (4) or (5) only need to be solved in the vicinity of the zero Level Set function, instead of in the whole domain. Therefore the effective computational cost of the method will vary with time and with the problem considered, but will always be bounded by  $N$ . Moreover, the Level Set method has proven to be particularly efficient in tracking interfaces of a sharply varying advected field, even in the presence of strong topological changes [Sethian, 1999, and references therein].

[23] In addition, this formulation allows a straightforward calculation of critical geometric quantities such as the unit normal vector to the interface:

$$\mathbf{n} = \frac{\nabla\phi}{|\nabla\phi|} \quad (8)$$

and the mean curvature:

$$\Gamma = \nabla \cdot \mathbf{n}, \quad (9)$$

which are required in order to evaluate surface tension acting on the interface  $\Omega$  [Brackbill et al., 1992]. This can be relevant to several geodynamic scenarios such as metal diapir fragmentation in a magma ocean during the earliest stages of terrestrial planet evolution [Rubie et al., 2003; Ichikawa et al., 2010] or gas bubble dynamics in magma flows [Manga

and Stone, 1994]. Note that additional useful geometric quantities can be derived from the Level Set such as the area of the interface  $\Omega$  [Sethian, 1999]. This important advantage of the Level Set method over Lagrangian advection is illustrated in Figure 1, which displays the surface tension magnitude and vectors of a 2D heterogeneity located in the center of a square domain discretized with  $100 \times 100$  identical cells. For simplicity we have considered a static problem, therefore advection is totally absent. However, the compositional field is either calculated using a Tracer-in-Cell method with 25 tracers/cell (Figures 1a and 1b), or using the Level Set method (Figures 1c and 1d). The surface tension is calculated using the Continuum Surface Force (CSF) formulation of Brackbill et al. [1992], involving second order derivatives of either  $\phi$  (for the Level Set method) or  $C$  (for the Tracer-in-Cell method) in the vicinity of the interface. To the naked eye, both Tracer-in-Cell and Level Set methods lead to indistinguishable compositional fields  $C$  (compare Figures 1a and 1c). However, the resulting surface tension (Figures 1b and 1d) are very different. The Tracer-in-Cell method yields incoherent direction, sign and magnitude of the surface tension (Figure 1b). This is a direct consequence of the discontinuity in  $C$ , which is well captured by the Tracer-in-Cell method, leading to numerical instabilities when determining the normal vectors  $\mathbf{n}$  and the curvature  $\Gamma$ . On the other hand, the use of a smooth function in the Level Set method allows accurate determination of the surface tension acting on the interface (Figure 1d). Of course, there are ways to limit these problems in Lagrangian methods, for instance by artificially smoothing  $C$  near the interface and by using first order differencing. However, this alters the accuracy of the solution.

[24] Despite its advantages, the Level Set method still suffers from inaccuracies due to numerical diffusion and dispersion (even though the use of a smooth function  $\phi$  significantly reduces the problem), artificial displacement of the zero Level Set during the reinitialization process, and does not allow efficient capture of sub-grid scale features [Suckale et al., 2010]. For these reasons, the Level Set method often fails to conserve mass accurately [Sussman et al., 1994; Enright et al., 2002]. We remark that on the contrary, Lagrangian methods are not affected by these particular difficulties.

## 2.2.2. Particle Level Set Method

[25] More recently, a Lagrangian improvement to the Level Set method was developed by Enright et

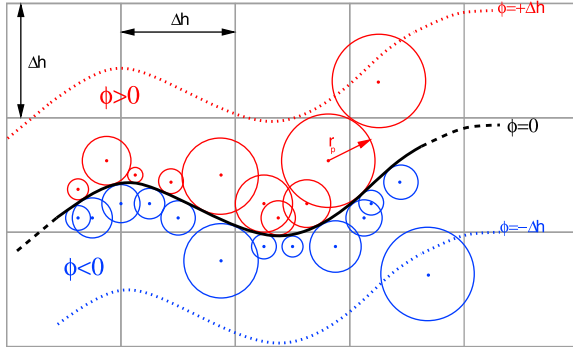


**Figure 2.** Schematic representation of the interface  $\Omega$  (zero Level Set) in the Particle Level Set method. The radius  $r_p$  of positive (red) and negative (blue) Lagrangian tracer particles of location  $\mathbf{x}_p$  are used to better track the evolution of zero Level Set.

*al.* [2002]. It consists of using Lagrangian tracer particles that are not prone to numerical diffusion to perform two sets of corrections to the Level Set in regions where its accuracy is low (i.e., mainly where the Level Set smoothness is low). Initially, as depicted in Figure 2, the tracers are randomly located at a distance  $\pm 3\Delta h = 3 \max(\Delta x, \Delta y, \Delta z)$  on both sides the zero Level Set. Each tracer particle is considered to be a sphere of radius  $r_p$  centered on  $\mathbf{x}_p$ , which defines locally the zero Level Set by being tangent to the interface (Figure 2). Therefore, in addition to their position  $\mathbf{x}_p$ , tracers carry two pieces of information: a sign  $s_p$ :  $-1$  for tracers initially located in regions where  $\phi < 0$ ,  $+1$  otherwise; and a “radius”  $r_p$ , which is the distance  $\phi(\mathbf{x}_p)$  between the tracer’s location and the zero Level Set.  $\phi(\mathbf{x}_p)$  is the local value of the Level Set at  $\mathbf{x}_p$  determined by linear interpolation, using the grid values of the closest neighboring points surrounding each tracer. Note that  $r_p$  is bounded by a minimum and a maximum value  $r_{\min}$  and  $r_{\max}$ , respectively:

$$r_p = \min(r_{\max}, \max(|\phi(\mathbf{x}_p)|, r_{\min})), \quad (10)$$

where we choose  $r_{\min} = 0.1 \min(\Delta x, \Delta y, \Delta z)$  and  $r_{\max} = 0.5 \min(\Delta x, \Delta y, \Delta z)$  as proposed by *Enright et al.* [2002]. We have tested other values, without noticeable improvement. Note that contrary to Tracer-in-Cell methods, here the tracer particles are considered to be massless, and are therefore allowed to overlap. In fact, an optimum tracking of the interface is obtained for tracer particles that closely overlap each other [*Enright et al.*, 2002].

[26] The first set of corrections aims to reduce the errors/inaccuracies in solving the Level Set equation (3). Tracers are used to reconstruct the

interface in those regions, identified as follows: positive particles that are found in the region  $E^+$  where the Level Set function is negative and conversely negative particles that are found in the region  $E^-$  where the Level Set function is positive, define regions where the Level Set needs to be corrected (Figure 3a).

[27] In order to reduce the errors the following corrections  $\phi^+$  and  $\phi^-$  are calculated in regions  $E^+$  and  $E^-$

$$\phi^+ = \max(\phi_p, \phi^+), \forall p \in E^+ \quad (11a)$$

$$\phi^- = \min(\phi_p, \phi^-), \forall p \in E^-, \quad (11b)$$

where  $\phi^+$  and  $\phi^-$  are first initialized to  $\phi$ , and  $\phi_p$  is a local Level Set function associated with each tracer particle:

$$\phi_p(\mathbf{x}) = s_p(r_p - |\mathbf{x} - \mathbf{x}_p|). \quad (12)$$

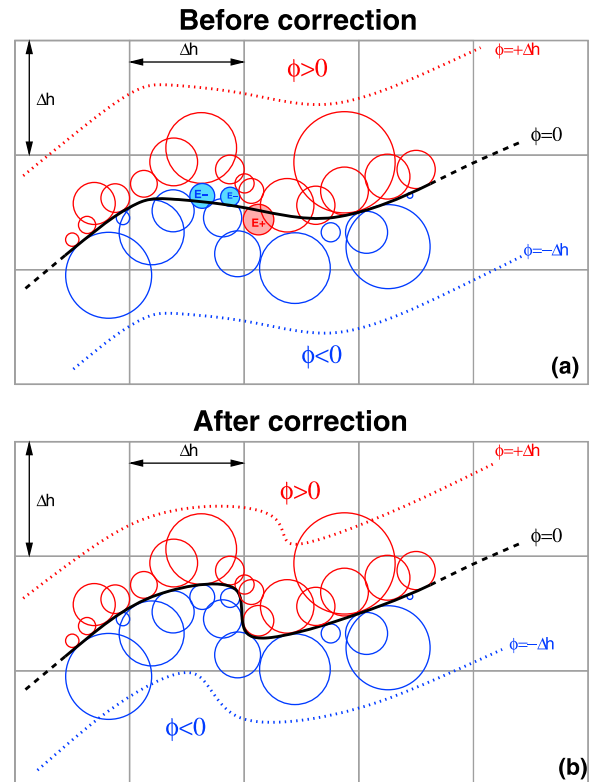


**Figure 3.** (a) Schematic representation of the Particle Level Set method prior to the correction step. Due to inaccuracies in solving the Level Set equation (3) positive (red) and negative (blue) particles have “escaped” and define  $E^+$  and  $E^-$  regions where the Level Set will be corrected. (b) Schematic representation of the Particle Level Set method after the correction step. See text for further explanation.

[28] Finally,  $\phi^+$  and  $\phi^-$  are merged back into a single, corrected Level Set by giving priority to values that are closer to the interface (Figure 3b):

$$\phi = \begin{cases} \phi^+ & \text{if } |\phi^+| \leq |\phi^-| \\ \phi^- & \text{if } |\phi^+| > |\phi^-| \end{cases} \quad (13)$$

[29] The second correction is applied to the Level Set in order to reduce the errors introduced in the reinitialization step (see section 2.2.1) during which the zero Level Set may have been erroneously displaced. Instead of correcting explicitly the reinitialized Level Set  $\phi$ , each tracer particle's radius  $r_p$  is readjusted according to equation (10) without altering the particle location. This "static" radius adjustment will favor the Level Set corrections performed on the next time step.

[30] The Particle Level Set algorithm can be summarized as follow:

[31] 1. Advect tracer particles by solving equation (2).

[32] 2. Solve the Level Set equation (3).

[33] 3. Apply a set of corrections to the Level Set function.

[34] 4. Reinitialize the Level Set by solving equation (4) or (5).

[35] 5. Adjust the particles radii according to equation (10) (i.e., implicit correction of the Level Set performed on the next time step).

[36] 6. Move to the next time step.

[37] In order to remain efficient, the above algorithm must be supplemented by particle re-seeding and deletion procedures. Indeed, as the Level Set evolves, the interface may stretch or be distorted by the flow. Consequently the number of tracer particles per cell in the vicinity of the zero Level Set (defined as  $|\phi| \leq 3 \Delta h = 3 \max(\Delta x, \Delta y, \Delta z)$ ) may decrease to 0, or on the contrary become unnecessarily high. It may also happen that tracer particles migrate too far away from the zero Level Set, where they become useless. Therefore, particles are deleted when they are found in regions where  $|\phi| > 3\Delta h$  or when they are located within the region  $|\phi| \leq 3\Delta h$  and their number per cell exceeds  $2N_{\text{tracer/cell}}$ . In addition, tracers are added in cells within the region  $|\phi| \leq 3\Delta h$  if the number per cell is 0. The cost involved in deletion/re-seeding procedures is similar to that involved in advecting the tracers particles. However, contrary to the steps listed in the Particle Level Set algorithm, the re-seeding and deletion procedures do not need to be performed at every

time step. As remarked by *Enright et al.* [2002], the frequency of re-seeding and deleting particles is problem dependent. In the examples presented in section 3 we find re-seeding and deleting every five time steps, as opposed to every time step, did not affect our results significantly. However, the computational savings can be substantial, in particular for 3D geometries. Finally, note that as long as there is at least one tracer per cell in the region  $|\phi| > 3\Delta h$ , re-seeding does not lead to numerical diffusion. This is due to the fact that for the Particle Level Set method, the location of the interface (determined by the corrected zero Level Set) is not affected by the addition or removal of tracer particles at a given time.

### 3. Comparison of the Numerical Methods for Advection in Geodynamic Flows

[38] We have set up a series of numerical experiments in 2D and 3D Cartesian geometries to test the accuracy and the efficiency of the Particle Level Set method. As a reference, we have chosen to compare these two methods with the Tracer-in-Cell approach only, because among the popular methods for solving equation (1), the Tracer-in-Cell method is probably one of the most robust and versatile.

[39] We first briefly describe the set of governing equations (in addition to equation (1)), which determine the velocity field  $\mathbf{U}$ : the conservation of mass, momentum and energy. This set of equations defines our geodynamic framework. Next we briefly describe the numerical methods used to solve the set of governing equations. This will be followed by comparisons of the methods for 2D and 3D geodynamic flows.

#### 3.1. Governing Equations and Numerical Methodology

[40] We consider here thermochemical convection of a Boussinesq viscous fluid in the limit of infinite Prandtl number. In this case, fluid motions  $\mathbf{U}$  may be described by the following set of dimensionless conservation equations for mass:

$$\nabla \cdot \mathbf{U} = 0, \quad (14)$$

the conservation of momentum:

$$\nabla p - \nabla \cdot \bar{\sigma} + (Ra T - Rb C)\bar{e}_z = 0, \quad (15)$$

and the conservation of energy:

$$\frac{\partial T}{\partial t} + \mathbf{U} \cdot \nabla T = \nabla^2 T, \quad (16)$$

where  $p$  is the dynamic pressure,  $T$  is the potential temperature,  $t$  is the time,  $\bar{\sigma}$  is the deviatoric viscous stress tensor, and  $\vec{e}_z$  is a unit vector along the vertical  $z$  axis. These equations are non-dimensionalized using the following characteristic scales: the thickness of the convective domain  $H$  for distances, the super-adiabatic temperature difference between the top and bottom surfaces  $\Delta T$  for temperature, and  $H^2/\kappa$  for time, where  $\kappa$  is the thermal diffusivity. The equation of state for the dimensionless density is:  $\rho = \rho_0 (1 - \alpha T + C \Delta \rho_c / \rho_0)$ , where  $\rho_0$  is the reference density,  $\alpha$  is the thermal expansion, and  $\Delta \rho_c = \rho (C = 1) - \rho (C = 0)$  is the compositional density contrast.

[41] The first non-dimensional number that appears in the conservation of momentum is a thermal Rayleigh number,  $Ra = \rho_0 \alpha \Delta T g H^3 / (\eta_0 \kappa)$ , where  $g$  is the gravitational acceleration and  $\eta_0$  is the reference viscosity. The second is a compositional Rayleigh number,  $Rb = \Delta \rho_c g H^3 / (\eta_0 \kappa)$ .

[42] The whole set of conservation equations is solved using a finite volume code StreamV3D. Two different approaches are used to solve the Stokes (mass and momentum) equations. In 2D, a pure stream function formulation is adopted [Samuel, 2009]. This reduces the set of Stokes equations to one biharmonic equation for the stream function that automatically satisfies the conservation of mass [e.g., Christensen, 1989; van Keken et al., 1997]. The stream function is calculated at nodal points, leading to a natural finite volume configuration where the velocity components are located at the center of each cell surface.

[43] For 3D cases, the mass and momentum equations are solved using a primitive variable formulation on a staggered grid with a SIMPLER algorithm [Patankar, 1980; Albers, 2000].

[44] The set of discretized Stokes equations is solved in 2D with a fast sparse direct solver (superLU [Demmel et al., 1999]) or with a robust iterative conjugate gradient method [Press et al., 1992] for cases with a large number of points.

[45] A finite volume formulation is used to discretize the energy equation (16) on a staggered grid [e.g., Patankar, 1980; Albers, 2000]. Two approaches are available for treating the advection term in equation (16) in StreamV3D: a pure Eulerian approach where a Total Variation Diminishing scheme with various flux limiters is used [Sweby,

1984; Roe, 1986], or the Tracer-in-Cell method [Gerya and Yuen, 2003; Samuel and Tackley, 2008]. However, in this paper the spatial derivatives in equation (16) are discretized using a pure Eulerian TVD scheme with Sweby a flux limiter [Sweby, 1984]. Time derivatives are approximated by explicit, first order finite differences subject to a Courant-Friedrich-Lewy stability criteria.

[46] Finally, equation (1) is either solved using the Particle-in-Cell or the Particle Level Set method. Unless specified otherwise, for tests with the Particle Level Set method, the Level Set equation (3) is discretized with the same finite volume TVD scheme with a Sweby flux limiter, as for the energy equation.

[47] The code has been successfully benchmarked against analytical solutions (see appendix A), purely thermal and thermo-chemical benchmarks [Blankenbach et al., 1989; van Keken et al., 1997] including strongly variable viscosity cases (see also section 3.2 and Appendix A).

### 3.2. Two-Dimensional Flows

[48] We consider the well-known thermochemical benchmarks presented by van Keken et al. [1997] in a 2D Cartesian box of aspect ratio  $\lambda$ , with different velocities and temperature boundary conditions and different values for  $Ra$  and  $Rb$ . The initial condition for the composition corresponds to a horizontally layered structure of thickness  $d_b$ . The time evolution of several quantities is monitored, in particular the Root Mean Square velocity:

$$V_{rms} = \sqrt{\frac{1}{V} \int \|\mathbf{U}\|^2 dV}, \quad (17)$$

and the entrainment  $e$  above a given dimensionless height  $d_e$ :

$$e = \frac{1}{\lambda^{n-1} d_b} \int_{z=d_e}^{z=1} C dV, \quad (18)$$

where  $n$  is the number of spatial dimensions. In addition, the mass error [Tackley and King, 2003] was monitored for each run:

$$\Delta M = \frac{(\int C dV)_t - (\int C dV)_{t=0}}{(\int C dV)_{t=0}}. \quad (19)$$

#### 3.2.1. Rayleigh-Taylor Benchmarks

[49] The first set of numerical experiments corresponds to a gravitational destabilization of a light layer of initial thickness  $d_b = 0.2$  in a 2D Cartesian

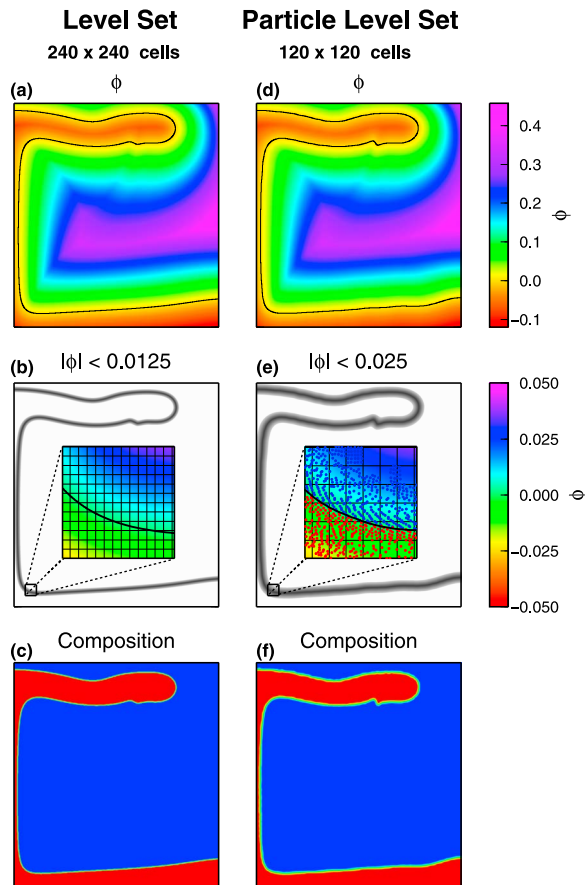


**Figure 4.** Comparison between (a–c) Level Set and (d–f) Particle Level Set methods in the case of the Rayleigh-Taylor benchmark with constant viscosity ( $\Delta\eta = 1$ ), at  $t = 500$ . Figures 4a and 4d show the Level Set  $\phi$ . The black contour delineates the interface between the two materials (i.e.,  $\phi = 0$ ). In Figures 4b and 4e the Level Set is shown in gray scale in the vicinity of the interface  $|\phi| < 3\Delta x = 3\Delta z = 3\Delta h$ . A zoom on a small region is displayed with the zero Level Set (black contour) and the local value of the Level Set  $\phi$ . For the Particle Level Set positive (red) and negative (blue) Lagrangian tracer particles are displayed in the zoom window (Figure 4e). Figures 4c and 4f show compositional field  $C$ . Red ( $C = 1$ ) corresponds to the light material initially overlaid by a dense viscous fluid represented in blue ( $C = 0$ ).

box of aspect ratio  $\lambda = 0.9142$ . In this case  $Ra$  is set to 0 and  $Rb$  to 1. Rigid, isothermal boundary conditions are applied on horizontal surfaces while the vertical surfaces are reflective. The layer is initially deflected by  $w = 0.02\cos(\pi x/\lambda)$ . Three cases are considered for which  $\Delta\eta$ , the ratio of the viscosity in the dense layer  $\eta_r$  to the reference viscosity  $\eta_0$ , is 1, 10 and 100.

[50] Before comparing the results obtained using the Tracer-in-Cell and the Particle Level Set

methods, we illustrate further the use of implicit surfaces in advecting a sharply varying scalar field  $C$ . Figure 4 shows the results of one Rayleigh-Taylor benchmark case with constant viscosity ( $\Delta\eta = 1$ ) at dimensionless time  $t = 500$ . Figures 4a–4c are obtained using the Level Set method on a  $240 \times 240$  cell grid while Figures 4d–4f are obtained using the Particle Level Set method on a  $120 \times 120$  cell grid. Figures 4a and 4d display the Level Set and the interface between the two materials is delineated by the black contour, representing  $\phi = 0$ . One can clearly see that the use of a signed distance function for the Level Set maintains a smooth field  $\phi$ . Although we advect and reinitialize the Level Set in the whole domain, which represents a computational cost of  $O(N)$ , this could be reduced by considering only a small region in the vicinity of the interface, defined as  $|\phi| \leq 3 \max(\Delta x, \Delta z)$ . As shown in Figures 4b and 4f, this can considerably reduce the computational cost, as the domain  $|\phi| \leq 3 \max(\Delta x, \Delta z)$  depicted in gray is only a small fraction of the entire grid. Zooming on a small region, displayed in Figures 4b and 4e, the Level Set and Particle Level Set methods differ in the use of positive (red) and negative (blue) Lagrangian tracer particles (Figure 4e) to apply corrections to the Level Set  $\phi$ . The Lagrangian particles also only need to be placed in the region  $|\phi| \leq 3 \max(\Delta x, \Delta z)$ . Figures 4c and 4e show the results of the Level Set conversion into a compositional field  $C$ , for the Level Set and Particle Level Set methods, respectively. The compositional field has preserved a very sharp variation across the interface. The  $C$  fields for both Level Set and Particle Level Set are very similar, however the Particle Level Set displays finer details despite the grid resolution being twice coarser than the one used for the Level Set method.

[51] Figure 5 shows the comparison between the Particle Level Set and the Tracer-in-Cell method for the three Rayleigh-Taylor benchmark cases (corresponding to  $\eta_0 = 1, 0.1$  and  $0.01$ ), at dimensionless time  $t = 1500$ , and for two grid resolutions ( $60 \times 60$  cells and  $120 \times 120$  cells). Although the results obtained with the Particle Level Set and Tracer-in-Cell methods show comparable global features, in detail, differences can be observed between the methods and between fine and coarse grid cell results. For instance, the heights of the rising plume heads observed for  $\Delta\eta = 1$  and  $\Delta\eta = 10$  on the coarse grid with the Tracer-in-Cell method (Figures 5a and 5e) are lower than what is found with the Particle Level Set method (Figures 5b and 5f). These differences between the Tracer-in-

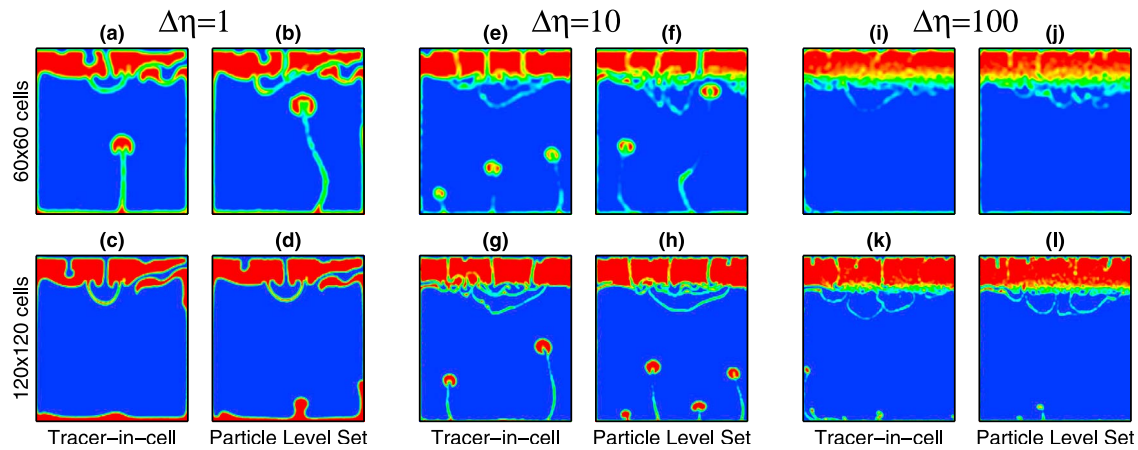


**Figure 5.** Results of the Rayleigh-Taylor benchmark: Compositional fields  $C$  at  $t = 1500$  for various viscosity ratios  $\Delta\eta = 1, 10, 100$ . Red ( $C = 1$ ) corresponds to the dense material and blue ( $C = 0$ ) corresponds to the light material. Figures 5a, 5b, 5e, 5f, 5i, and 5j correspond to a  $60 \times 60$  cells grid while Figures 5c, 5d, 5g, 5h, 5k, and 5l display the results obtained on a  $120 \times 120$  cells grid. The results obtained with Tracer-in-Cell and the Particle Level Set methods are displayed. Compare with Figures 2, 4 and 6 of *van Keken et al.* [1997] and Figure 1 of *Tackley and King* [2003].

Cell and Particle Level Set method are reduced on the finer grid. Such discrepancies between methods were also observed in previous studies for the same benchmark [*van Keken et al.*, 1997; *Tackley and King*, 2003]. As theory predicts, the growth rate of Rayleigh-Taylor instability is exponential [*Chandrasekhar*, 1961]. Therefore, even small differences between the methods are exponentially amplified with time.

[52] The time evolution of  $V_{\text{rms}}$  and the entrainment  $e$  above 0.2 for the three benchmark cases for the Particle Level Set method on a  $120 \times 120$  cell grid, using 25 tracers per cell are displayed in Figures 6a and 6b, respectively. These quantities compare well with the results published by *van Keken et al.* [1997] and *Tackley and King* [2003], which shows that the Particle Level Set method allows an accurate reproduction of the Rayleigh-Taylor benchmarks.

[53] We have performed tests to investigate the minimum number of tracers per cell  $N_{\text{tracer/cell}}$  necessary to model advection accurately with the Particle Level Set method. Results are displayed in Figure 7 that shows the maximum absolute value of the mass error  $M$  calculated during the Rayleigh-Taylor benchmark with  $\Delta\eta = 100$  as a function of  $N_{\text{tracer/cell}}$  for three different grid resolutions. When  $N_{\text{tracer/cell}} = 0$  (i.e., using the pure Eulerian Level Set method) the mass error can be very large, on the order of several tens of percent. Note however that this could significantly be reduced if extension velocities were used to advect the Level Set [*Sethian*, 1999; *Adalsteinsson and Sethian*, 1999; *Suckale et al.*, 2010]. Using only one tracer/cell

reduces mass errors to 1–2%. Finally, for  $N_{\text{tracer/cell}} \geq 4$  mass errors are reduced to an acceptable level (i.e.,  $\leq 1\%$ ) for any grid size. Again using extension velocities or a more accurate reinitialization of the Level Set one could reasonably expect that even

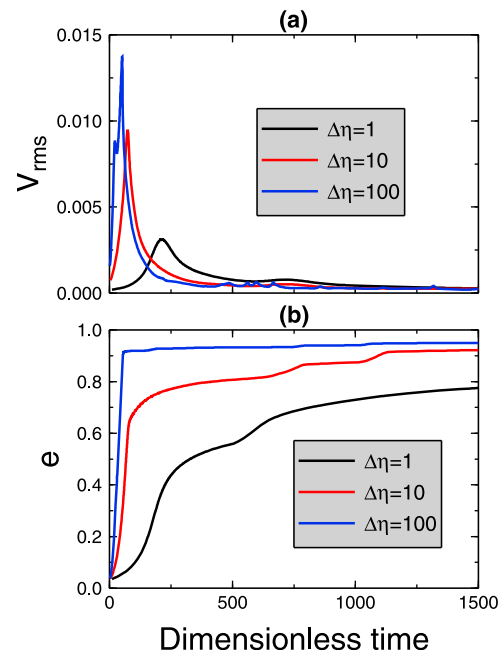


**Figure 6.** Results for the Particle Level Set method. Time evolution of (a) the RMS velocity and (b) the entrainment above  $z = 0.2$  for the Rayleigh-Taylor benchmark with various viscosity ratios. Compare with Figures 3, 5 and 7 of *van Keken et al.* [1997] and Figure 2 of *Tackley and King* [2003].

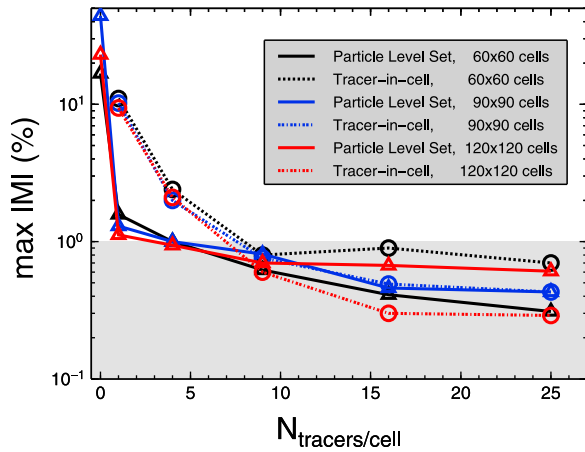


**Figure 7.** Results for the Rayleigh-Taylor benchmark with a viscosity ratio  $\Delta\eta = 100$ . Maximum value of the mass error for various grid resolutions as a function of the number of tracer particles per cell, for both the Tracer-in-Cell (dashed line and circles) and the Particle Level Set (solid lines and triangles) methods. The gray area represents the domain where the mass is reasonably well conserved (i.e.,  $\max IMI < 1\%$ ).

smaller values of  $N_{\text{tracer/cell}}$  necessary to model advection accurately with the Particle Level Set method. This should be investigated in the future. For comparison we have displayed in Figure 7 similar curves obtained with the Tracer-in-Cell method. Larger values of  $N_{\text{tracer/cell}}$  (i.e., 9) are necessary to reduce mass errors below 1%. Overall, we

verified with all the 2D and 3D cases presented in this paper the following rules of thumb for the minimum value of  $N_{\text{tracer/cell}}$  required in order to conserve mass accurately in a domain with  $n$  spatial dimensions:

$$\text{Particle Level Set} : N_{\text{tracer/cell}} \geq 2^n \quad (20a)$$

$$\text{Tracer-in-Cell} : N_{\text{tracer/cell}} \geq 3^n. \quad (20b)$$

The above rules are compatible with previous studies using the Tracer-in-Cell method [van Keken *et al.*, 1997; Tackley and King, 2003; Gerya and Yuen, 2003] and Particle Level Set method [Enright *et al.*, 2002, 2005].

[54] Additional selected quantities for these cases with various grid resolutions are listed in Table 1. The values obtained with the Particle Level Set or the Tracer-in-Cell method compare well with those listed in van Keken *et al.* [1997] and Tackley and King [2003]. In addition, both methods conserve mass within less than 1% for any grid size. For reference we have included in Table 1 several cases calculated with the Level Set method, which illustrates that mass conservation for the pure Eulerian Level Set method is more problematic and requires higher grid resolution.

[55] Figure 8 shows the computational time spent for advecting the compositional field  $t_{\text{adv}}$  normal-

**Table 1.** Selected Quantities for the Rayleigh-Taylor Benchmark Problems<sup>a</sup>

Method	Grid	Growth Rate $\gamma$	$t$ (max $V_{\text{rms}}$ )	max $V_{\text{rms}}$	max $ \Delta MI (\%)$	mean $ \Delta MI (\%)$
$\Delta\eta = 1$						
Level Set	60 × 60	0.006607	228.88	0.002925	4.51	2.29
Level Set	120 × 120	0.011066	215.87	0.003051	1.68	0.66
Level Set	240 × 240	0.011519	211.52	0.003093	0.04	0.02
Particle Level Set	60 × 60	0.010643	215.57	0.003087	0.56	0.12
Particle Level Set	120 × 120	0.011549	212.22	0.003109	0.18	0.04
Tracer-in-Cell	60 × 60	0.011143	213.72	0.003135	0.14	0.05
Tracer-in-Cell	120 × 120	0.011953	214.04	0.003129	0.07	0.03
$\Delta\eta = 10$						
Level Set	60 × 60	0.040860	78.48	0.009087	3.03	1.14
Level Set	120 × 120	0.044414	75.89	0.009269	1.72	0.59
Level Set	240 × 240	0.046040	73.45	0.009480	0.18	0.07
Particle Level Set	60 × 60	0.046090	71.98	0.009375	0.83	0.24
Particle Level Set	120 × 120	0.046034	74.07	0.009414	0.63	0.10
Tracer-in-Cell	60 × 60	0.043853	75.86	0.009193	0.34	0.10
Tracer-in-Cell	120 × 120	0.046188	72.54	0.009185	0.31	0.59
$\Delta\eta = 100$						
Level Set	60 × 60	0.09787	55.81	0.01212	3.67	1.37
Level Set	120 × 120	0.10309	51.33	0.01414	0.64	0.20
Level Set	240 × 240	0.10359	50.65	0.01445	0.27	0.09
Particle Level Set	60 × 60	0.10477	51.06	0.01360	0.98	0.44
Particle Level Set	120 × 120	0.10354	51.09	0.01405	0.84	0.23
Tracer-in-Cell	60 × 60	0.10343	52.90	0.01292	0.52	0.30
Tracer-in-Cell	120 × 120	0.10138	51.23	0.01392	0.33	0.16

<sup>a</sup>For the cases calculated with the Particle Level Set and Tracer-in-Cell method, 25 tracers per cell are used.

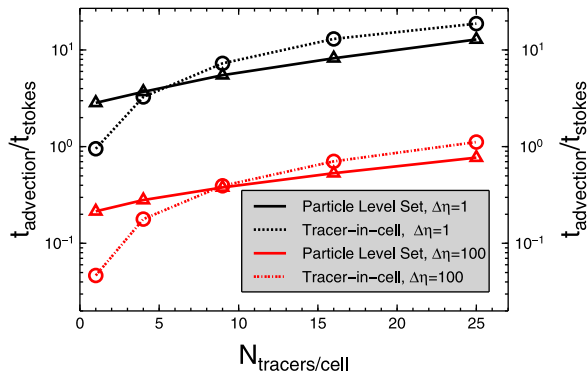


**Figure 8.** Computational cost involved in solving the advection equation (1) for the Rayleigh-Taylor benchmark using  $60 \times 60$  grid cells, for either a viscosity ratio  $\Delta\eta = 100$  (red) or for constant viscosity (black). The Tracer-in-Cell (dotted curves and circles) and Particle Level Set (solid curves and triangles) methods are compared as a function of the numbers of tracers/cell used. The computational costs are normalized by  $t_{\text{Stokes}}$ , the computational time involved in solving the Stokes equations. Here about 600 and 1250 uneven time steps were necessary to reach the final time  $t = 2500$  for  $\Delta\eta = 1$  and 100, respectively.

ized by  $t_{\text{Stokes}}$ , the time spent solving the Stokes equations. For small amounts of tracers per cell the computational cost involved in advection is larger for the Particle Level Set method than for the Tracer-in-Cell method. However, for  $N_{\text{tracer/cell}} \geq 9$  (recall that this is also the minimum value recommended for the Tracer-in-Cell method in 2D according to equation (20b)) the Particle Level Set method is more efficient than the Tracer-in-Cell method. For instance, for  $N_{\text{tracer/cell}} = 9$  and  $\Delta\eta = 1$ , the Particle Level Set method is about 30% faster than the Tracer-in-Cell method. The efficiency of the Particle Level Set method over the Tracer-in-Cell is even more pronounced if one considers that a smaller value of  $N_{\text{tracer/cell}}$  is required for the Particle Level Set method, as previously discussed (Figure 7 and equation (20)). Taking this into account the Particle Level Set method is at least  $\sim 30$  to 100% faster than the Tracer-in-Cell method. Further improvement in efficiency for the Particle Level Set method would be achieved by solving the Level Set equation only in the vicinity of the interface (as opposed to the whole domain as we do here). It is also interesting to remark that in these 2D benchmarks even for variable viscosity, advection represents a significant fraction of the computational time (at least 15 to 20% for variable viscosity, and more for constant viscosity). Therefore in these experiments reducing the time spent

for advecting the compositional field will make a significant impact on the overall calculation time.

### 3.2.2. Entrainment of a Thin Dense Layer

[56] Here, with  $Ra = 3 \cdot 10^5$ ,  $Rb = 4.5 \cdot 10^5$  and  $\lambda = 2$  we consider the entrainment of a dense layer of initial thickness  $d_b = 0.025$ , with constant viscosity. An analytical initial condition for temperature is prescribed (see *van Keken et al.* [1997] for the exact expression). The horizontal surfaces are free slip and isothermal and the vertical sidewalls are reflective.

[57] For this benchmark we present results obtained on a  $120 \times 60$  cell grid for the Tracer-in-Cell and the Particle Level Set methods, with 25 tracers/cell. Figure 9 displays a comparison between compositional fields at several dimensionless times  $t$  obtained using the Tracer-in-Cell and the Particle Level Set methods for solving equation (1). The two methods yield very similar results until  $t = 0.02$ , after which the evolution diverges slightly. Note that the Particle Level Set method does not suffer from spurious statistical noise present in the Tracer-in-Cell method. Indeed, while fluctuations in the composition  $C$  within the dense layer are visible in Figure 9 (left) at  $t = 0.01$ , they are absent in Figure 9 (right) at  $t = 0.01$ .

[58] Figure 10 displays the time evolution of  $V_{\text{rms}}$  and the entrainment  $e$  above 0.2 and shows a good quantitative agreement between the Particle Level Set and the Tracer-in-Cell methods. Similar to previous studies [*van Keken et al.*, 1997; *Samuel and Farnetani*, 2003; *Tackley and King*, 2003] for  $t > 0.02$  results tend to diverge between the two methods, probably due to the chaotic nature of the flow where small divergences are exponentially amplified with increasing time. Therefore we can conclude that here again the Particle Level Set method allows an accurate reproduction of the thermochemical entrainment benchmark.

[59] We have tested the influence of the accuracy of the numerical scheme for discretizing equation (3). In agreement with *Enright et al.* [2005], the results displayed in Figure 11 clearly show that higher order spatial (fifth order WENO) and temporal (third order Runge-Kutta) discretization yield very similar results for both velocities (Figure 11a) and entrainment (Figure 11b). In addition, in Figure 12a we have compared the time evolution of the entrainment  $e$  above  $z = 0.2$  obtained with the Particle Level Set method using various flux limiters. Similarly, the choice of the flux limiter does

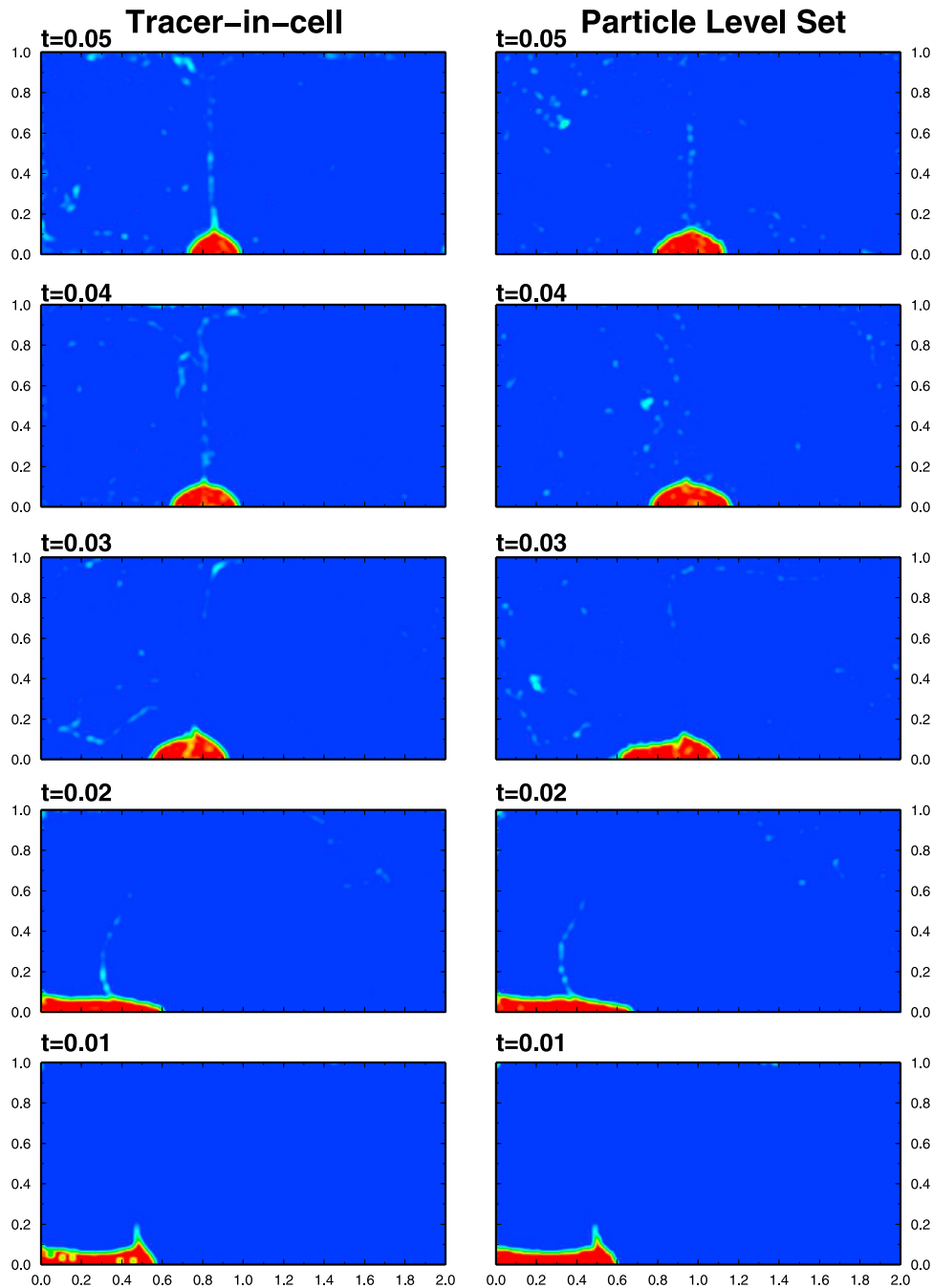


**Figure 9.** Results of the entrainment layer benchmark: five snapshots in time of the Compositional fields  $C$  obtained using (left) the Tracer-in-Cell and (right) the Particle Level Set methods.

not lead to substantial differences. This is mainly due to the fact that the level set is smooth, therefore the flux limiters are not really “activated” in the vicinity of the interface. This is clearly shown in Figure 12a where the entrainment obtained without using a flux limiter (basic centered scheme) is similar to cases that use a flux limiter for solving the Level Set equation (3). In addition, the presence

of tracer particles would also tend to minimize possible differences between various flux limiters.

[60] We performed convergence tests to investigate the effect of the number of tracers per cell used for the Particle Level Set method on the entrainment  $e$  above  $z = 0.2$ . Results, shown in Figure 12b indicate that for fine grids  $N_{\text{tracer/cell}}$  has a weak influence on the entrainment (as long as  $N_{\text{tracer/cell}} > 0$ ).

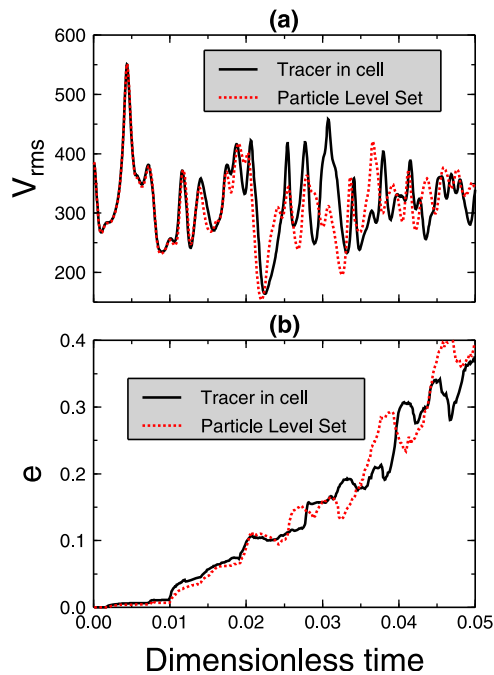


**Figure 10.** Results of the entrainment layer benchmark. Time evolution of (a) the RMS velocity and (b) the entrainment above  $z = 0.2$  obtained using the Tracer-in-Cell and the Particle Level Set methods. Compare with Figure 12 of *van Keken et al.* [1997] and with Figure 4 of *Tackley and King* [2003].

This means that only one tracer per cell is sufficient to resolve accurately sub-grid scale features with the Particle Level Set method. However, this is not a sufficient condition since, as pointed out in section 3.2.1 and in Figure 7, at least 4 tracers per cell are needed to reduce mass errors to less than 1% in 2D.

[61] Note that with such a small initial layer thickness  $d_b$ , sub-grid scale resolution is critical for this benchmark problem. This is partly the reason why Eulerian approaches fail to reproduce this benchmark [*van Keken et al.*, 1997] (in addition to diffusion and dispersion errors). To illustrate this further, we have performed experiments with the pure Eulerian Level Set method (i.e., no tracers) and find that even on a  $240 \times 120$  grid the entrainment  $e$  above  $z = 0.2$  is almost zero, throughout the whole calculation. This underestimation of the entrainment is a direct consequence of the fact that pure Eulerian Level Set fails to capture sub-grid scale features, as shown by *Suckale et al.* [2010]. The ability to resolve sub-grid scales represents certainly one of the most attractive advantages of the Particle Level Set method compared to other Eulerian approaches, including the pure Eulerian Level Set method itself.

[62] In summary, the comparisons performed between implicit surfaces and Tracer-in-Cell methods for 2D flows have shown that the Particle Level Set method can yield similar results to the Tracer-in-Cell method at the same grid resolution. This includes cases where sub-grid scale resolution is critical.

### 3.3. Three-Dimensional Flows

[63] Advection in three-dimensional flows is computationally expensive, in particular when using Lagrangian methods. Therefore we have conducted 3D experiments to compare the accuracy and the computational efficiency of the Tracer-in-Cell and the Particle Level Set methods.

[64] We have selected three geodynamic problems, the first two involving strong topological changes in  $C$  and sub-scale flow that are particularly difficult to model accurately. In these problems, pure Eulerian methods solving equation (1) would auto-

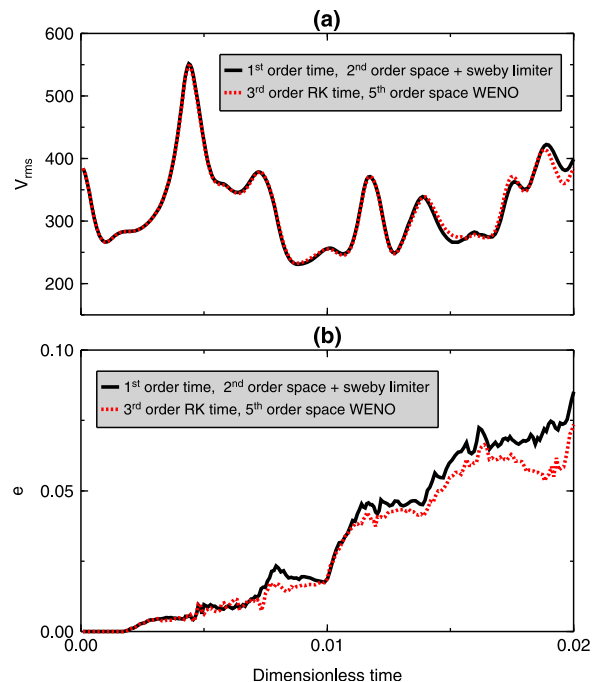


**Figure 11.** Results of the entrainment layer benchmark with the Particle Level Set method on a  $120 \times 60$  cell with 25 tracers/cell. Comparison between the results obtained using high order time and space discretization (third order TVD Rung Kutta and fifth order WENO scheme for spatial derivatives, red dashed curves) and results obtained with a lower accuracy (black curves) for both time (first order explicit) and space (second order TVD with Sweby flux limiter). Time evolution of (a) the RMS velocity and (b) the entrainment above  $z = 0.2$ .

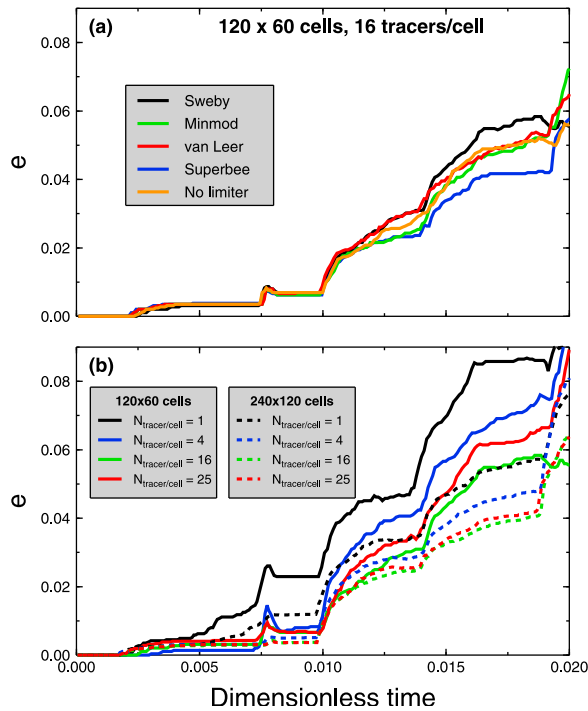


**Figure 12.** Results of the entrainment layer benchmark with the Particle Level Set method. Time evolution of the entrainment above  $z = 0.2$ . (a) Influence of the flux limiters applied for solving equation (3) on a  $120 \times 60$  cell with 16 tracers/cell. (b) Convergence test with two grid resolutions and various numbers of tracers/cell.

matically fail to compare well with the more robust Lagrangian (e.g., Tracer-in-Cell) methods. For all cases presented in this section, we use 27 tracers/cell for both the Tracer-in-Cell and Particle Level Set methods.

### 3.3.1. Convective Stirring of a Passive Heterogeneity

[65] We consider the homogenization via convective stirring of a passive heterogeneity in a  $1 \times 1 \times 1$  domain discretized using  $60 \times 60 \times 60$  grid cells. The horizontal surfaces are free-slip and isothermal and the vertical walls are reflective. The values of the governing parameters are  $Ra = 10^7$  and  $Rb = 0$ . The initial temperature condition, shown in Figure 13a was obtained after reaching a statistical steady state. At  $t = 0$  a spherical passive heterogeneity ( $C = 1$ ) of dimensionless radius 0.25 is placed in the center of the domain, while the composition in the surrounding fluid is initialized to  $C = 0$  (Figure 13b). The calculation is run for several thousand time steps, which would scale for the Earth to a few billion years.

[66] Figure 14 displays snapshots in time of the iso-surface  $C = 0.5$  and of a horizontal cut at mid-depth obtained by solving equation (1) with the Tracer-in-Cell (left) or the Particle Level Set (right) methods. Despite the strong topological changes due to the repeated action of convective stretching and folding, the results obtained with both methods agree very well. This remains true even in the late stages, where the compositional field becomes more homogeneous.

[67] The time evolution of the composition is also monitored via histograms that show the distribution of  $C$  at dimensionless time corresponding to the snapshots displayed in Figure 15. The histograms obtained with the Tracer-in-Cell and Particle Level

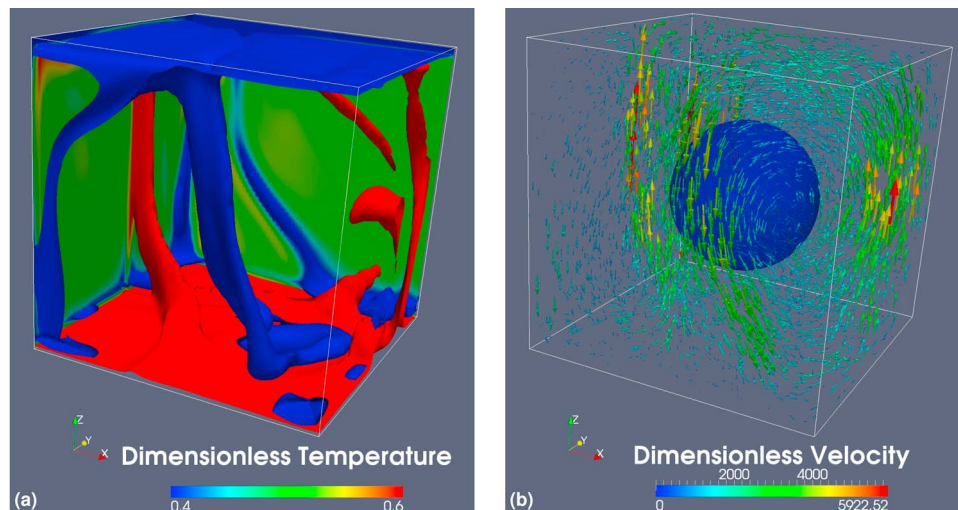


**Figure 13.** Initial condition for the 3D passive convective stirring test. (a) Dimensionless temperature  $T$ . (b) Dimensionless velocity field (arrows) and iso-contour displaying the interface between the passive heterogeneity and the surrounding mantle.

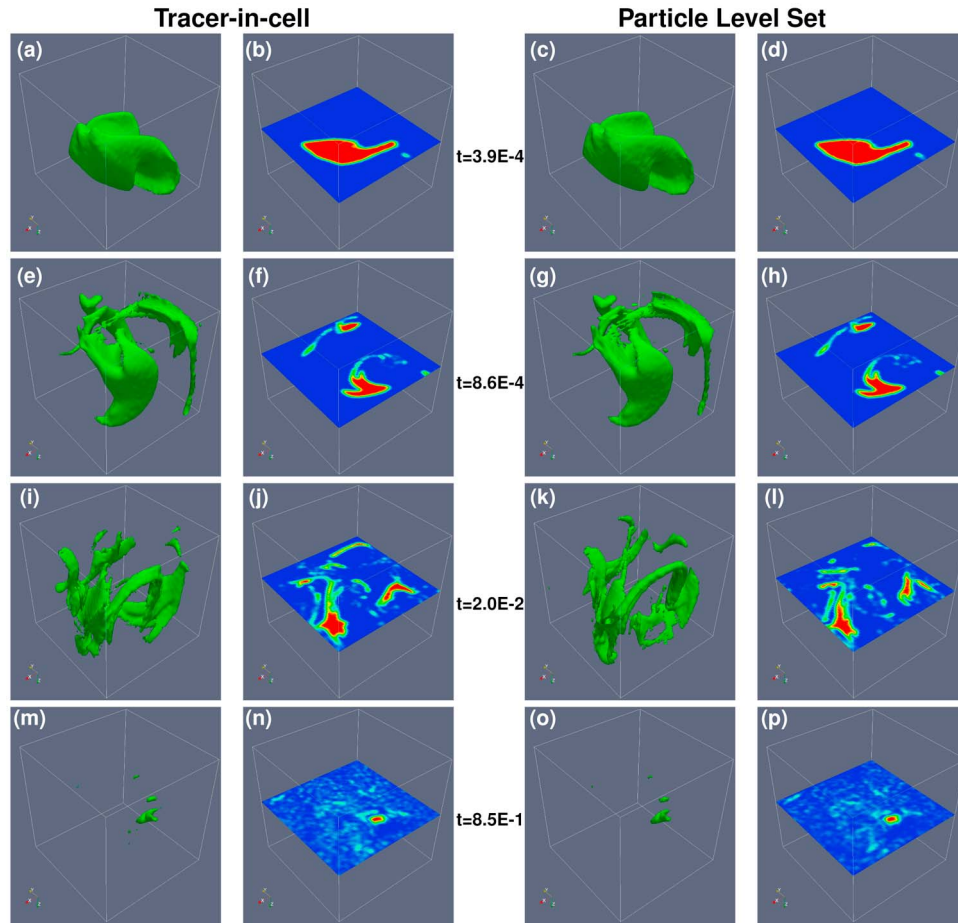


**Figure 14.** Results of the 3D passive convective stirring test. Comparison of the time evolution of the passive compositional field  $C$  obtained with the Tracer-in-Cell and the Particle Level Set methods. Iso-contours corresponding to  $C = 0.5$  (green) and a mid-depth surface cut are shown.

Set method also agree very well. They both show that the  $C$  distribution evolves towards a Gaussian shape as a result of vigorous convective stirring.

[68] This first 3D test demonstrates the ability of the Particle Level Set method to compete with robust Tracer-in-Cell advection. Moreover, the Particle Level Set method allows a significant reduction in computational time because only tracers near the interface are involved, contrary to the Tracer-in-Cell method where tracers are located everywhere in the computational domain. Nevertheless, in this particular example the computational gain of using the Particle Level Set method decreases with time because the area occupied by the zero Level Set increases exponentially with time as a result of convective stirring. Consequently, the number of tracers particles used to correct the Level Set increases. However, this increase is bounded by the total number of grid cells, and stabilizes around an asymptotic value  $N_{\text{trmax}} \sim N \times$

$N_{\text{tracer/cell}}$ , corresponding ultimately to a fully homogenized state.

### 3.3.2. Destabilization of a Dense Layer

[69] We consider the homogenization via convective stirring of a passive heterogeneity in a  $2 \times 2 \times 1$  domain discretized using  $60 \times 60 \times 30$  grid cells. The horizontal surfaces are free-slip and isothermal and the vertical walls are reflective. The values of the governing parameters are  $Ra = 10^7$  and  $Rb = 2 \cdot 10^6$ . Similar to the previous case, the initial temperature condition was obtained after running a convection calculation until reaching a statistical steady state. At  $t = 0$  a dense layer of dimensionless thickness 0.3 ( $C = 1$ ) is placed in the bottom of the domain, while the composition in the overlying fluid is initialized to  $C = 0$ . The calculation is run until complete destabilization and homogenization of the dense layer is achieved.

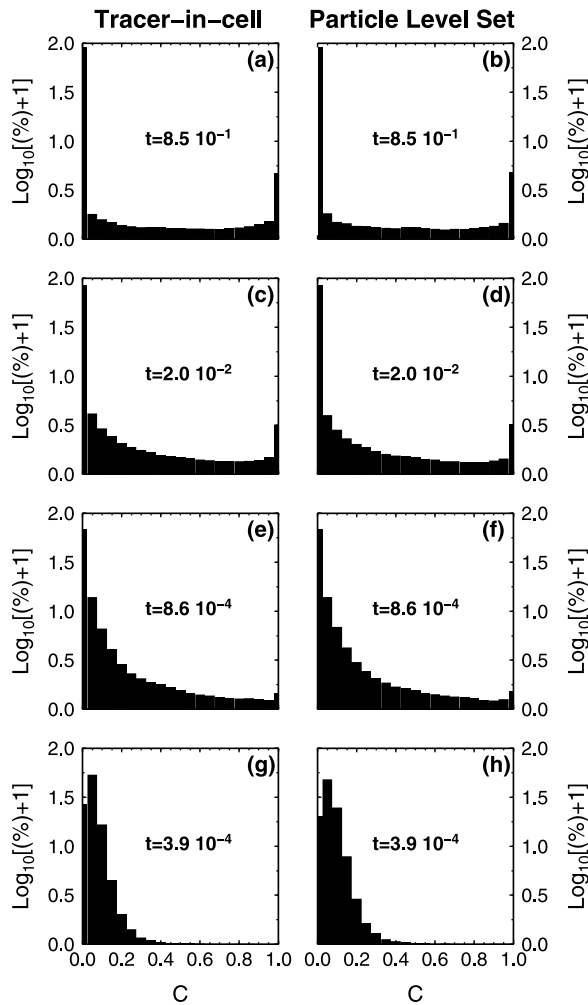


**Figure 15.** Results of the 3D passive convective stirring test. Comparison of the time evolution of the passive compositional field  $C$  obtained with the Tracer-in-Cell and the Particle Level Set methods. The histograms represent the distribution of the compositional field  $C$  within the computational domain. The  $C$  distribution evolves towards a Gaussian shape as a result of vigorous convective stirring. The dimensionless time  $t$  correspond to the snapshots displayed in Figure 14.

[70] Figure 16 displays four snapshots in time of the iso-surface  $C = 0.5$  and transparent surface cuts for cases where equation (1) is solved with the Tracer-in-Cell (Figures 16a, 16c, 16e, and 16g) or the Particle Level Set (Figures 16b, 16d, 16f, and 16h) methods. The dense layer gets progressively heated by the bottom surface until the thermal density contrast overcomes the compositional density contrast. After this stage is reached the dense layer rapidly forms a topography (Figures 16a and 16b) and large domes of dense material rise up and are stirred by convective motions (Figures 16c–16g).

The comparison of the Particle Level Set and Tracer-in-Cell cases are in good qualitative agreement, and the results obtained with both methods agree very well. A more quantitative comparison between the results obtained with the Tracer-in-Cell and Particle Level Set the methods is shown in Figure 17, which displays the time evolution of the entrainment  $e$  above  $z = 0.3$ . As expected from the dynamic evolution observed in Figure 16, the entrainment increases rapidly as the dense layer is destabilized and reaches the asymptotic value of 0.7 corresponding to the complete homogenization of the heterogeneous material. Both the Particle Level Set and Tracer-in-Cell methods yield very similar results. Further comparison can be made using the composition histograms displayed in Figure 18 at four different elapsed times corresponding to the snapshots shown in Figure 16. The distribution evolves

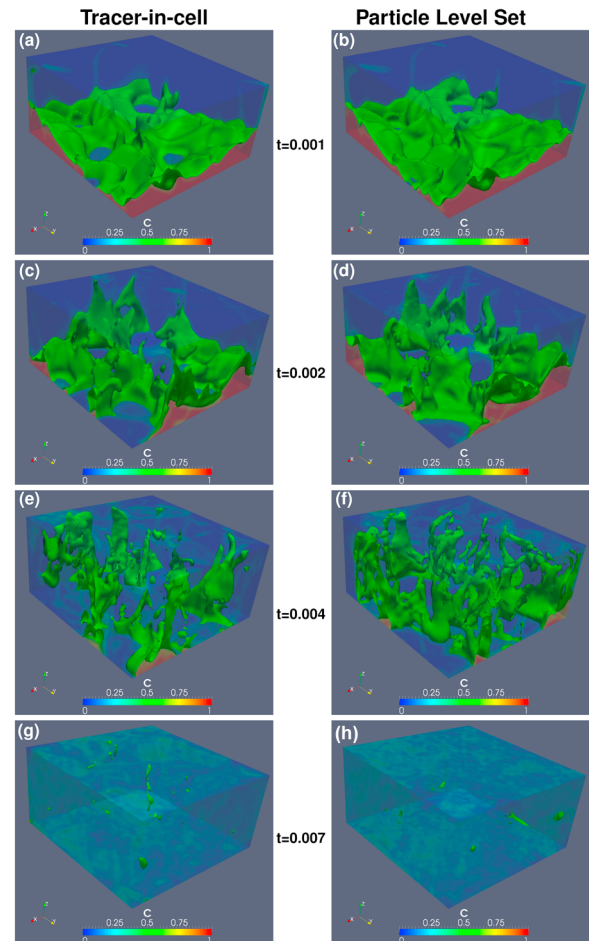


**Figure 16.** Results of the 3D destabilization of a thick dense layer test. Comparison of the time evolution of the passive compositional field  $C$  obtained with the Tracer-in-Cell and the Particle Level Set methods. Iso-contours corresponding to  $C = 0.5$  (green).

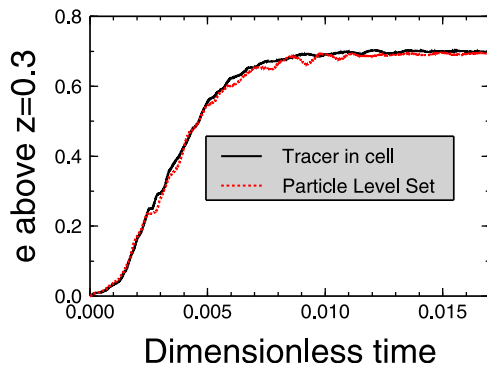


**Figure 17.** Results of the 3D destabilization of a thick dense layer test. Time evolution of the entrainment above  $z = 0.3$  obtained using the Tracer-in-Cell (solid black curve) and the Particle Level Set (dashed red curve) methods.

towards a Gaussian shape as a result of the ergodicity. Here again, comparison of the Particle Level Set and Tracer-in-Cell cases are in very good quantitative agreement, even in the late stages.

[71] Both three-dimensional flow experiments have clearly demonstrated the ability of the Particle Level Set method to model accurately the advection of sharply varying fields even in the case of vigorous thermal or thermo-chemical convective stirring, where the repeated action of stretching and folding leads to the development of filament structures that can reach sub-grid scale. Despite these difficulties, the results obtained with the Particle Level Set method are in remarkably good agreement with those obtained with the robust Tracer-in-Cell method. However, the Particle Level Set method allows for a significant reduction in computational cost ( $\sim 50\%$ ) compared to the Tracer-in-Cell method. Note that in terms of computational expenses, the two examples selected represent the least favorable scenarios for the Particle Level Set method because they lead to complete homogenization where the zero Level Set is present in every cell. As a consequence, tracers associated with the interface will also be located everywhere in the computational domain, similar to the Tracer-in-Cell method.

### 3.3.3. Buoyant Compositional Plume

[72] Following *Manga et al.* [1993], *Schmalzl and Loddoch* [2003], and *Suckale et al.* [2010], we have performed a 3D experiment where we model the rise of a buoyant compositional (i.e.,  $Ra = 0$ ) plume using the Particle Level Set method, in a  $45 \times 45 \times 45$  grid of aspect ratio 1. Initially the light material is a half-sphere of dimensionless radius 1,

located at the bottom of the domain. The compositional Rayleigh number is  $Rb = 0.15$ . Time is non-dimensionalized using the Stokes velocity time scale [*Manga et al.*, 1993], all boundaries are free-slip. Figure 19 shows snapshots in time of the plume which compare well with the numerical experiments of *Manga et al.* [1993], *Schmalzl and Loddoch* [2003], and *Suckale et al.* [2010] and the tank experiments of *Manga et al.* [1993].

[73] Contrary to the two previous 3D experiments, the Particle Level Set method here is particularly efficient to use, because the interface spans a rela-

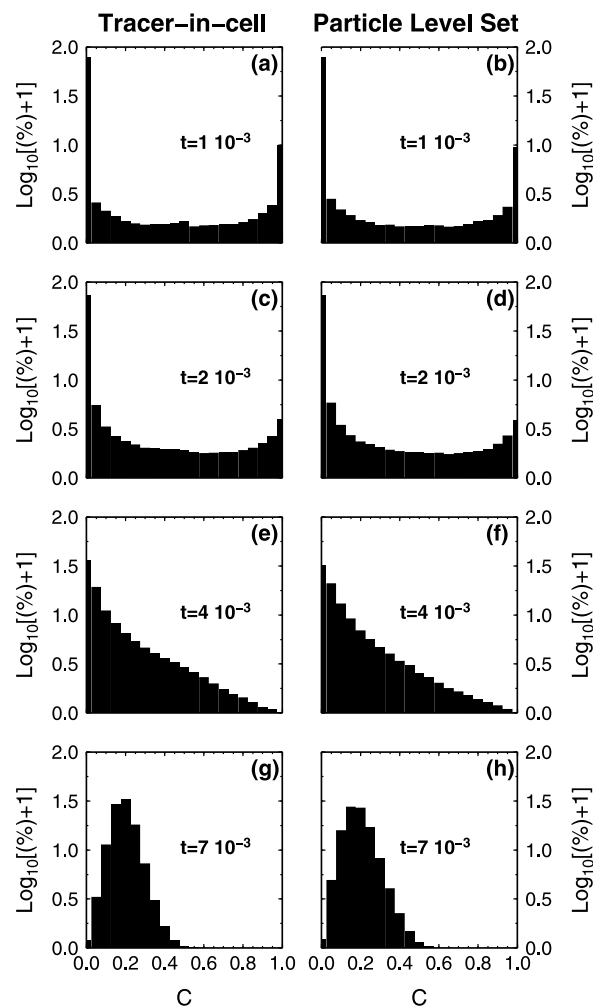


**Figure 18.** Results of the 3D destabilization of a thick dense layer test. Comparison of the time evolution of the passive compositional field  $C$  obtained with the Tracer-in-Cell and the Particle Level Set methods. The histograms represent the distribution of the compositional field  $C$  within the computational domain. As in Figure 15, the  $C$  distribution evolves towards a Gaussian shape as a result of vigorous convective stirring. The dimensionless time  $t$  correspond to the snapshots displayed in Figure 16.

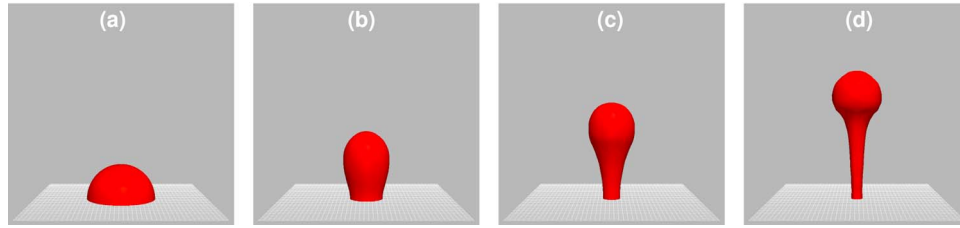


**Figure 19.** Time evolution of a light compositional plume rising up from a free-slip surface [Manga *et al.*, 1993; Schmalzl and Loddoch, 2003; Suckale *et al.*, 2010] calculated with the Particle Level Set method on a  $45 \times 45 \times 45$  cells grid with 27 tracers per cell. Iso-surfaces of the zero Level Set at four dimensionless times: (a)  $t = 0$ , (b)  $t = 8.4$ , (c)  $t = 16.8$ , (d)  $t = 25.2$ .

tively small fraction of the model domain, discretized using  $N$  cells. This is illustrated in Figure 20 where the computational cost involved in solving the advection equation (1) using the Tracer-in-Cell or the Particle Level Set methods on a  $30 \times 30 \times 30$  grid are compared, for various values of  $N_{\text{tracers/cell}}$ . As expected, for both methods  $t_{\text{adv}}$  scales linearly with  $N_{\text{tracers/cell}}$ , however,  $t_{\text{adv}}$  is 4 to 10 times smaller for the Particle Level Set method because tracer particles are only located in the vicinity of the interface, contrary to the Tracer-in-Cell method for which tracers are located everywhere in the model domain. Note that for finer grids, the ratio  $t_{\text{adv}}/t_{\text{Stokes}}$  would decrease, however the gain in using the Particle Level Set method instead of the Tracer-in-Cell approach would remain substantial.

#### 4. Conclusions

[74] We have adapted for the first time a robust numerical method for advecting scalar fields with discontinuities in geodynamical thermochemical flows: the Particle Level Set method. This approach is a Lagrangian extension of the Level Set method based on the concept of dynamic implicit surfaces, that allows the use of accurate and stable high order schemes, even in areas where the advected field varies sharply. The improved Eulerian-Lagrangian character of the Particle Level Set method yields more accurate solutions for the advection of sharply varying quantities.

[75] We have compared the accuracy and robustness of the Particle Level Set method with the popular and robust Tracer-in-Cell method in 2D and 3D flows: Rayleigh-Taylor overturn, thermochemical convection, mantle convective stirring, and the rise of a buoyant compositional plume.

[76] For all 2D and 3D cases, the results obtained with the Particle Level Set and the Tracer-in-Cell

method are in very good quantitative agreement, even in the case of 3D chaotic convective stirring and for cases where sub-grid scale resolution is critical. The Particle Level Set method is accurate, prone to negligible numerical diffusion, and can capture sub-grid scale features. In most cases the Particle Level Set method is significantly faster than the Tracer-in-Cell method as it requires the use of tracer particles only in the vicinity of interfaces. For instance, we observed a one order of magnitude reduction in computational expenses in solving equation (1) for tests where the interface does not span the whole computational domain. This demonstrates the robustness, versatility and the computational efficiency of the Particle Level Set method. We therefore recommend the use of the Particle Level Set method for any geodynamical

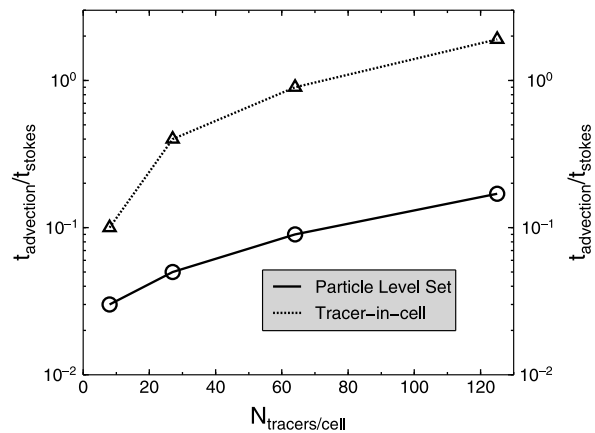


**Figure 20.** Computational cost involved in solving the advection equation (1) for the plume problem using  $30 \times 30 \times 30$  grid cells. The Tracer-in-Cell (dotted curves and triangles) and Particle Level Set (solid curves and circles) methods are compared as a function of the numbers of tracers/cell used. The computational costs are normalized by  $t_{\text{Stokes}}$ , the computational time involved in solving the Stokes equations.

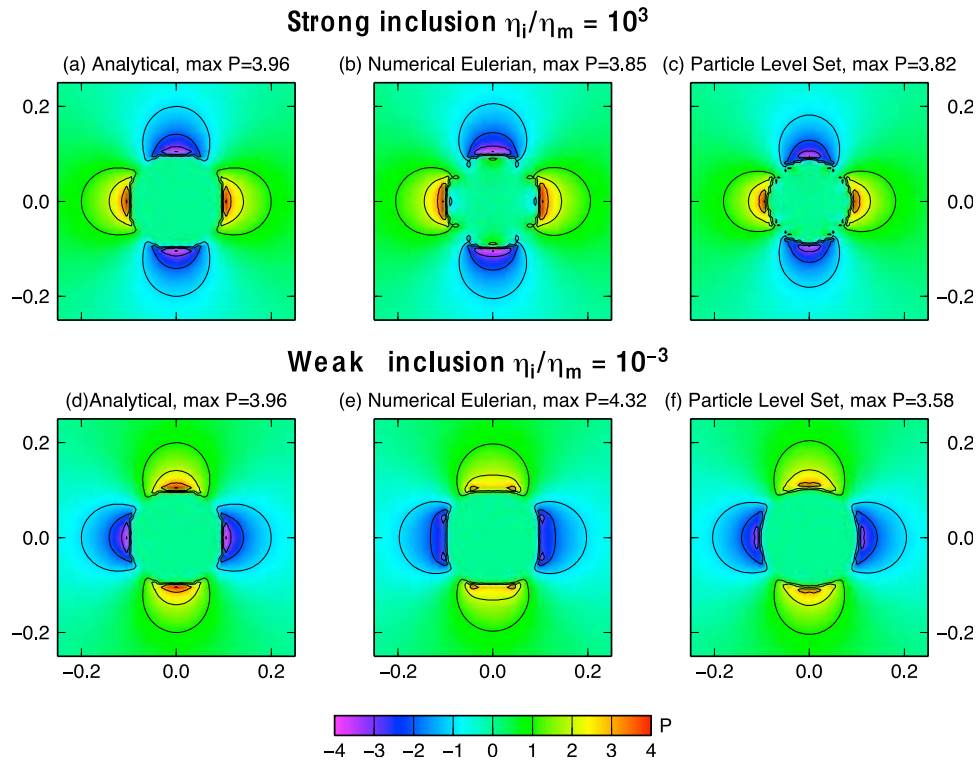


**Figure A1.** Circular inclusion benchmark test in a pure shear flow [Deubelbeiss and Kaus, 2008]. Instantaneous pressure field calculated in a pure shear flow containing a circular inclusion of dimensionless radius 0.1 and of viscosity  $\eta_i$  different from the surrounding matrix  $\eta_m = 1$ . (a) Analytical solution of Schmid and Podladchikov [2003] for a strong inclusion, (b) corresponding numerical solution obtained with a pure Eulerian (i.e., field) approach, and (c) numerical solution obtained with the Particle Level Set method using 9 tracers per cell. The black curves mark the isocontours of  $P = \{-4, -3, -2, -1, 1, 2, 3, 4\}$ . The benchmark setup and resolution is identical to that shown in the Figure 10 of Deubelbeiss and Kaus [2008]. (d–f) Similar to Figures A1a–A1c but for a weak inclusion.

cal problem that involves the pure advection of sharply varying quantities.

## Appendix A: Flow Solver Benchmark

[77] In order to test the accuracy of our flow solver, we have performed a benchmark comparison with the analytical solution of Schmid and Podladchikov [2003], as proposed by Deubelbeiss and Kaus [2008]. The problem consists of calculating the instantaneous flow field in a domain where the pure shear boundary conditions of Schmid and Podladchikov [2003] are applied on the four boundaries. In addition, a circular inclusion of viscosity  $\eta_i$  of dimensionless radius  $r_i = 0.1$  is located in the center of the domain. The dimensionless surrounding matrix viscosity  $\eta_m$  is 1. The inclusion is either weak ( $\eta_i/\eta_m < 1$ ) or strong ( $\eta_i/\eta_m > 1$ ). Schmid and Podladchikov [2003] have derived analytical solutions for this problem, one of which is shown in Figure A1a for the case of a

strong inclusion with  $\eta_i/\eta_m = 1000$ . Figure A1b displays the numerical solution calculated with a pure Eulerian (field) approach, using  $280 \times 280$  nodal points, the same resolution used in the Figure 10 of Deubelbeiss and Kaus [2008]. The agreement between numerical and analytical solutions is good: the maximum pressure calculated is 2.8% lower than the analytical solution, which is smaller than the 11% difference found by Deubelbeiss and Kaus [2008] for the same conditions. Figure A1c displays the numerical solution calculated with a Particle Level Set method with 9 tracers per cell, which yields very similar results to those shown in Figure A1b. As observed by Deubelbeiss and Kaus [2008] the use of tracer particles helps to reduce the spurious oscillations present in the vicinity of the interface, where the error is maximum. In addition, we calculate the Root Mean Square error defined as:

$$RMS_{\text{error}} = \sqrt{\frac{\int_{\text{domain}} (P_{\text{numeric}} - P_{\text{analytic}})^2}{N \int_{\text{domain}} P_{\text{analytic}}^2}}, \quad (\text{A1})$$

where  $N$  is the total number of grid points used. We find that  $RMS_{\text{error}} = 0.13\%$  and  $0.18\%$  for the results displayed in Figures A1e and A1f, respectively. These values also compare well with the results of *Deubelbeiss and Kaus* [2008].

[78] Such a comparison has also been carried out in *Suckale et al.* [2010], except that they considered a weak inclusion with  $\eta_i/\eta_m = 10^{-3}$ . We have therefore performed the same tests. The analytical and numerical solutions are displayed in Figures A1d, A1e and A1f). We find a larger error (yet acceptable) for the maximum pressure than in the strong inclusion test, and comparable rms error values:  $RMS_{\text{error}} = 0.15\%$  and  $0.12\%$  for the results displayed in Figures A1e and A1f, respectively.

[79] As noted by *Deubelbeiss and Kaus* [2008], the good agreement between numerical and analytical solutions is mainly due to the combination of staggered grid and harmonic averaging of viscosities from cell centers to nodal points. Indeed, we find that geometric or arithmetic averaging of viscosities systematically yields larger differences between numerical and analytical solutions.

[80] These tests demonstrate the robustness of our Stokes solver for large viscosity contrasts.

## Acknowledgments

[81] The authors are grateful to Peter van Keken and an anonymous reviewer for their thoughtful suggestions, which significantly improved the manuscript. Henri Samuel acknowledges the funds from the Stifterverband für die Deutsche Wissenschaft. 2D figures were made with the Generic Mapping Tools [Wessel and Smith, 1995]. 3D figures were drawn with ParaView software.

## References

- Adalsteinsson, D., and J. A. Sethian (1999), The fast construction of extension velocities in level set methods, *J. Comput. Phys.*, *148*, 2–22.
- Albers, M. (2000), A local mesh refinement multigrid method for 3-D convection problems with strongly variable viscosity, *J. Comput. Phys.*, *160*(1), 126–150.
- Blankenbach, B., et al. (1989), A benchmark comparison for mantle convection codes, *Geophys. J. Int.*, *98*(1), 23–38.
- Brackbill, J. U., D. B. Kothe, and C. Zemach (1992), A continuum method for modeling surface tension, *J. Comput. Phys.*, *100*, 335–354.
- Chandrasekhar, S. (1961), *Hydrodynamic and Hydromagnetic Stability*, 643 pp., Dover, New York.
- Chemia, Z., H. Koyi, and H. Schmeling (2008), Numerical modelling of rise and fall of a dense layer in salt diapirs, *Geophys. J. Int.*, *172*, 798–816.
- Christensen, U. R. (1989), Mixing by time-dependent convection, *Earth Planet. Sci. Lett.*, *95*, 382–394.
- Christensen, U. R., and A. W. Hofmann (1994), Segregation of subducted oceanic crust in the convecting mantle, *J. Geophys. Res.*, *99*, 19,867–19,884.
- Demmel, J. W., S. C. Eisenstat, J. R. Gilbert, X. S. Li, and J. W. Liu (1999), A supernodal approach to sparse partial pivoting, *SIAM J. Matrix Anal. Appl.*, *20*, 720–755.
- Deubelbeiss, Y., and B. J. Kaus (2008), Comparison of Eulerian and Lagrangian numerical techniques for the Stokes equations in the presence of strongly varying viscosity, *Phys. Earth Planet. Inter.*, *171*, 92–111.
- Enright, D., R. Fedkiw, J. Ferziger, and I. Mitchell (2002), A hybrid particle level set method for improved interface capturing, *J. Comput. Phys.*, *183*(1), 83–116.
- Enright, D., F. Lossaso, and R. Fedkiw (2005), A fast and accurate semi-Lagrangian particle level set method, *Comput. Surf.*, *83*, 479–490.
- Farnetani, C. G., and M. A. Richards (1995), Thermal entrainment and melting in mantle plumes, *Earth Planet. Sci. Lett.*, *136*, 251–267.
- Farnetani, C. G., and H. Samuel (2003), Lagrangian structures and stirring in the Earth's mantle, *Earth Planet. Sci. Lett.*, *206*, 335–348.
- Farnetani, C. G., and H. Samuel (2005), Beyond the thermal plume paradigm, *Geophys. Res. Lett.*, *32*, L07311, doi:10.1029/2005GL022360.
- Fletcher, C. A. J. (1991), *Computational Techniques for Fluid Dynamics*, 401 pp., Springer, New York.
- Gerya, T. V., and D. A. Yuen (2003), Characteristics-based marker-in-cell method with conservative finite-differences schemes for modeling geological flows with strongly variable transport properties, *Phys. Earth Planet. Inter.*, *140*, 293–318.
- Gross, L., L. Bourgouin, A. J. Hale, and H.-B. Muhlhaus (2007), Interface modeling in incompressible media using level sets in Escript, *Phys. Earth Planet. Inter.*, *163*, 23–34.
- Harten, A. (1984), On a class of high resolution total-variation-stable finite-difference schemes, *SIAM J. Numer. Anal.*, *21*, 1–23.
- Harten, A., B. Engquist, S. Osher, and S. R. Chakravarthy (1987), Uniformly high order accurate essentially non-oscillatory schemes, III, *J. Comput. Phys.*, *71*, 231–303.
- Hořnk, T., J. Schmalzl, and U. Hansen (2006), Dynamics of metal-silicate separation in a terrestrial magma ocean, *Geochem. Geophys. Geosyst.*, *7*, Q09008, doi:10.1029/2006GC001268.
- Ichikawa, H., S. Labrosse, and K. Kurita (2010), Direct numerical simulation of an iron rain in the magma ocean, *J. Geophys. Res.*, *115*, B01404, doi:10.1029/2009JB006427.
- Lenardic, A., and W. M. Kaula (1993), Numerical treatment of geodynamic viscous-flow problems involving the advection of material interfaces, *J. Geophys. Res.*, *98*, 8243–8260.
- Lin, J.-R., T. V. Gerya, P. J. Tackley, D. A. Yuen, and G. J. Golabek (2009), Numerical modeling of protocore destabilization during planetary accretion: Methodology and results, *204*, 732–748.
- Lin, S.-C., and P. E. van Keken (2005), Multiple volcanic episodes of flood basalts caused by thermochemical mantle plumes, *Nature*, *436*, 250–252.
- Lin, S.-C., and P. E. van Keken (2006), Deformation, stirring and material transport in thermochemical plumes, *Geophys. Res. Lett.*, *33*, L20306, doi:10.1029/2006GL027037.
- Liu, X.-D., S. Osher, and T. Chan (1994), Weighted essentially non-oscillatory schemes, *J. Comput. Phys.*, *115*, 200–212.

- Manga, M. (1996), Mixing of chemical heterogeneities in the mantle: Effect of viscosity differences, *Geophys. Res. Lett.*, *23*, 403–406.
- Manga, M., and H. Stone (1994), Interactions between bubbles in magmas and lavas: Effects of bubble deformation, *J. Volcanol. Geotherm. Res.*, *63*, 267–279.
- Manga, M., H. Stone, and R. O’Connell (1993), The interaction of plume heads with compositional discontinuities in the Earth’s mantle, *J. Geophys. Res.*, *98*, 19,979–19,990.
- Ménard, T., S. Tanguy, and A. Berlemont (2007), Coupling level set/VOF/ghost fluid methods: Validation and application to 3D simulation of the primary break-up of a liquid jet, *Int. J. Multiphase Flow*, *33*, 510–524.
- Min, C., and F. Gibou (2007), A second order accurate level set method on non-graded adaptive cartesian grids, *J. Comput. Phys.*, *225*, 300–321.
- Monteux, J., Y. Ricard, N. Coltice, F. Dubuffet, and M. Ulvrova (2009), A model of metal-silicate separation on growing planets, *Earth Planet. Sci. Lett.*, *287*, 353–362.
- Muehlhaus, H.-B., L. Moresi, B. Hobbs, and D. F. (2002), Large amplitude folding in finely layered viscoelastic rock structures, *Pure Appl. Geophys.*, *159*, 2311–2333.
- Osher, S., and R. Fedkiw (2003), *Level Set Methods and Dynamic Implicit Surfaces*, 273 pp., Springer, New York.
- Osher, S., and J. A. Sethian (1988), Fronts propagating with curvature-dependent speed: Algorithms based on Hamilton-Jacobi formulations, *J. Comput. Phys.*, *79*, 12–49.
- Patankar, S. V. (1980), *Numerical Heat Transfer and Fluid Flow*, 197 pp., Hemisphere, New York.
- Press, W. H., S. A. Teukolsky, W. Vetterling, and B. P. Flannery (1992), *Numerical Recipes*, 933 pp., Cambridge Univ. Press, Cambridge, U. K.
- Ricard, Y., O. Sramek, and F. Dubuffet (2009), A multi-phase model of runaway core-mantle segregation in planetary embryos, *Earth Planet. Sci. Lett.*, *284*, 144–150.
- Roe, P. L. (1986), Characteristic-based schemes for the Euler equations, *Annu. Rev. Fluid Mech.*, *18*, 337–365.
- Rubie, D. C., H. J. Melosh, J. E. Reid, C. Liebske, and K. Righter (2003), Mechanisms of metal-silicate equilibration in the terrestrial magma ocean, *Earth Planet. Sci. Lett.*, *205*, 239–255.
- Samuel, H. (2009), STREAMV: A fast, robust and modular numerical code for modeling various 2D geodynamic scenarios, annual report, pp. 203–205, Bayerisches Geoinst., Bayreuth, Germany.
- Samuel, H., and D. Bercovici (2006), Oscillating and stagnating plumes in the Earth’s lower mantle, *Earth Planet. Sci. Lett.*, *248*, 90–105.
- Samuel, H., and C. G. Farnetani (2003), Thermochemical convection and helium concentrations in mantle plumes, *Earth Planet. Sci. Lett.*, *207*, 39–56.
- Samuel, H., and P. J. Tackley (2008), Dynamics of core formation and equilibration by negative diapirism, *Geochem. Geophys. Geosyst.*, *9*, Q06011, doi:10.1029/2007GC001896.
- Samuel, H., P. J. Tackley, and M. Evonuk (2010), Heat partitioning during core formation by negative diapirism in terrestrial planets, *Earth Planet. Sci. Lett.*, *290*, 13–19.
- Schmalzl, J., and A. Loddock (2003), Using subdivision surfaces and adaptive surface simplification algorithms for modeling chemical heterogeneities in geophysical flows, *Geochem. Geophys. Geosyst.*, *4*(9), 8303, doi:10.1029/2003GC000578.
- Schmalzl, J., G. A. Houseman, and U. Hansen (1996), Mixing in vigorous, time-dependent three-dimensional convection and application to Earth’s mantle, *J. Geophys. Res.*, *101*, 21,847–21,858.
- Schmelting, H., et al. (2008), A benchmark comparison of spontaneous subduction models—Towards a free surface, *Phys. Earth. Planet. Inter.*, *171*, 198–223.
- Schmid, D. W., and Y. Y. Podladchikov (2003), Analytical solutions for deformable elliptical inclusions in general shear, *Geophys. J. Int.*, *155*, 269–288.
- Sethian, J. A. (1999), *Level Set Methods and Fast Marching Methods*, Cambridge Univ. Press, Cambridge, U. K.
- Shu, C.-W., and S. Osher (1988), Efficient implementation of essentially non-oscillatory shock-capturing schemes, *J. Comput. Phys.*, *77*, 439–471.
- Smolakiewicz, P. K. (1984), A fully multidimensional positive definite advection algorithm with small implicit diffusion, *J. Comput. Phys.*, *54*, 325–362.
- Suckale, J., J.-C. Nave, and B. H. Hager (2010), It takes three to tango: 1. Simulating buoyancy-driven flow in the presence of large viscosity contrasts, *J. Geophys. Res.*, *115*, B07409, doi:10.1029/2009JB006916.
- Sussman, M., and E. Puckett (2000), A coupled level set and volume-of-fluid method for computing 3D and axisymmetric incompressible two-phase flows, *J. Comput. Phys.*, *162*, 301–337.
- Sussman, M., P. Smereka, and S. Osher (1994), A level set approach for computing solutions to incompressible two-phase flow, *J. Comput. Phys.*, *114*, 146–159.
- Sweby, P. K. (1984), High resolution schemes using flux limiters for hyperbolic conservation laws, *SIAM J. Numer. Anal.*, *21*, 995–1011.
- Tackley, P. J. (2002), Strong heterogeneity caused by deep mantle layering, *Geochem. Geophys. Geosyst.*, *3*(4), 1024, doi:10.1029/2001GC000167.
- Tackley, P. J., and S. D. King (2003), Testing the tracer ratio method for modeling active compositional fields in mantle convection simulations, *Geochem. Geophys. Geosyst.*, *4*(4), 8302, doi:10.1029/2001GC000214.
- van Hunen, J., A. P. van den Berg, and N. J. Vlaar (2004), Various mechanisms to induce present-day shallow flat subduction and implications for the younger Earth: A numerical parameter study, *Phys. Earth. Planet. Inter.*, *146*, 179–174.
- van Keken, P. E., S. D. King, H. Schmelting, U. R. Christensen, D. Neumeister, and M.-P. Doin (1997), A comparison of methods for the modeling of thermochemical convection, *J. Geophys. Res.*, *102*, 22,477–22,495.
- van Keken, P. E., C. J. Ballentine, and E. Hauri (2003), Convective mixing in the Earth’s mantle, in *Geochemistry of the Mantle and Core*, edited by K. K. Turekian and H. D. Holland, pp. 471–491, Elsevier, New York.
- Verhoeven, J., and J. Schmalzl (2009), A numerical method for investigating crystal settling in convecting magma chambers, *Geochem. Geophys. Geosyst.*, *10*, Q12007, doi:10.1029/2009GC002509.
- Weinberg, R. F., and H. Schmelting (1992), Polydiapirs: Multiwavelength gravity structures, *J. Struct. Geol.*, *4*, 425–436.
- Wessel, P., and W. H. F. Smith (1995), *Eos Trans. AGU*, *76*, 329.